Self-weight buckling of thin elastic shells: the case of a spherical equatorial segment

Ciprian D. Coman[1†]

[1] *Department of Computer Science, School of Computing & Engineering, University of Huddersfield, HD1 3DH, Huddersfield, UK*

October 12, 2022

Abstract

Buckling of an equatorial shallow shell segment under its own weight is re-considered here from a novel point of view involving singular-perturbation techniques. A number of different asymptotic approximations for the critical buckling load are proposed and discussed in detail, while comparisons with direct numerical simulations of the associated boundary-value problem confirm the excellent accuracy of the results obtained.

Keywords: shallow shells, eigenvalue problems, localised deformations, boundary layers, WKB approximations.

[†] cdc3p@yahoo.com

1 Introduction

Broadly speaking, the role of gravitational forces in the study of elastic instabilities experienced by traditional thin-walled structures is often ignored because of its secondary importance. Standard texts in the area of elastic buckling (e.g., [1, 2]) tend to limit their discussion vis-à-vis self-weight buckling as the sole cause of instability, perhaps with the exception of the so-called 'heavy elastica'. This phrase usually refers to a slender configuration (e.g., a flexible rod, a ribbon, etc.), whose overall weight qualifies as a major contender among other potentially destabilizing factors. Assuming a constant mass density for an elastic material (i.e., the weight of a structure made of such a material is proportional to its volume), the key question of interest in this context involves extremising some of the geometrical characteristics of the considered structure so that it remains in neutral equilibrium (e.g., [3]). A simple case in point is a vertical cylindrical rod fixed at the lower end and free at the top; here one would be interested in the maximum length for which the rod maintains a straight vertical shape; alternatively, if the length is prescribed, another possible question of interest would boil down to identifying the minimum cross-sectional radius for which the previous property holds true as well. This problem was first solved by Greenhill [4] in connection to how tall a tree can grow (for related and more recent work see [5, 6, 7]).

Interest in heavy elastica goes back to Leonhard Euler [8], who was one of the first to "wrestle" with formulating correct differential equations for a compressed vertical rod taking into account its weight (e.g., see [9] for interesting historical commentary). The corresponding buckling equations turn out to be mathematically more challenging than those for compressed rods having uniform mechanical properties and negligible weight, a fact that has mainly to do with the presence of variable coefficients and the absence of closed-form expressions for the corresponding buckling modes. Many of the proposed solutions in the literature have relied on power series (the Frobenius method), reduction to special functions (e.g., Bessel, Lommel, etc.), or direct numerical integration. Nevertheless, the current literature pertaining to this topic is vast and a thorough review is beyond the scope of this study. We will be content mentioning the short review by Wang [10] as well as the more recent and modern account given by Atanackovic [11] (e.g., see pp. 144-160).

Applications of self-weight buckling to practical problems are readily found in many branches of engineering. For example, Kerr [12] investigated the stability of a water tower consisting of a spherical vessel attached to the top of a tall vertical column. His simplified model was based on a variation of the heavy elastica, while also accounting for the flexibility of the column, the own weight of the structure, the weight of the liquid mass, as well as the rotational stiffness of the soil base. The role played by self-weight in the mechanical behaviour of shell structures tends to be more difficult to assess and requires large-scale computational models. For industrial (hyperbolic) cooling towers this aspect has been explored by Cole *et al.* [13] and Jullien *et al.* [14]. A similar analysis for cylindrical shells based on several shell theories was carried out by Lim & Ma [15]. References [16, 17, 18] provide ample information on the stress distributions in typical shell geometries subjected to gravity loads, and contain numerous pointers to the relevant literature on engineering applications.

In the oil & gas industry, the major component of rotary drilling systems is the so-called *drillstring* (e.g., see [19, 20]). This corresponds to a slender rod-like configuration formed by connecting together (many) individual thick-walled pipes (called *drill collars*); their outer diameters can range between 3 and 12 inches, and usually have a length of about 30 feet. As it is well documented (e.g., see [21] and the references therein), drillstrings are prone to buckling even though they are not directly subjected to compressive forces. In fact, their weight is partially supported by an applied tensile force at the top of the borehole; depending on the magnitude of this force one can control the amount of compression exerted on the lower part of the drillstring, which in turn is responsible for potential

buckling instabilities. Thus, ignoring the weight of the drillstring is not an option in this scenario. An interesting account of mathematical modelling of buckling instabilities in drillstring was recently given by Gulyayev *et al.* [22], to which the interested reader is referred for further information.

In a couple of interesting studies motivated by aerospace applications, Blum & McComb [23, 24] considered the elastic instability of an equatorial segment of a spherical shell loaded by its own weight; the corresponding situation is illustrated in Figure 1. The spherical segment seen there is symmetric with respect to the equatorial plane, it has height L, radius R, and uniform thickness h ($0 < h/R \ll 1$). This configuration is also assumed to be geometrically *shallow*, in the sense that the equatorial segment is more like a cylinder rather than a sphere (i.e., $0 < L/R \ll 1$). Both circular edges are taken to be simply supported, and its weight is balanced by uniformly distributed vertical line loads as seen in the right sketch included in the same Figure. One of the key questions of interest vis-à-vis this configuration is finding the critical thickness of the spherical segment so that it will be able to support its weight (without experiencing any buckling).

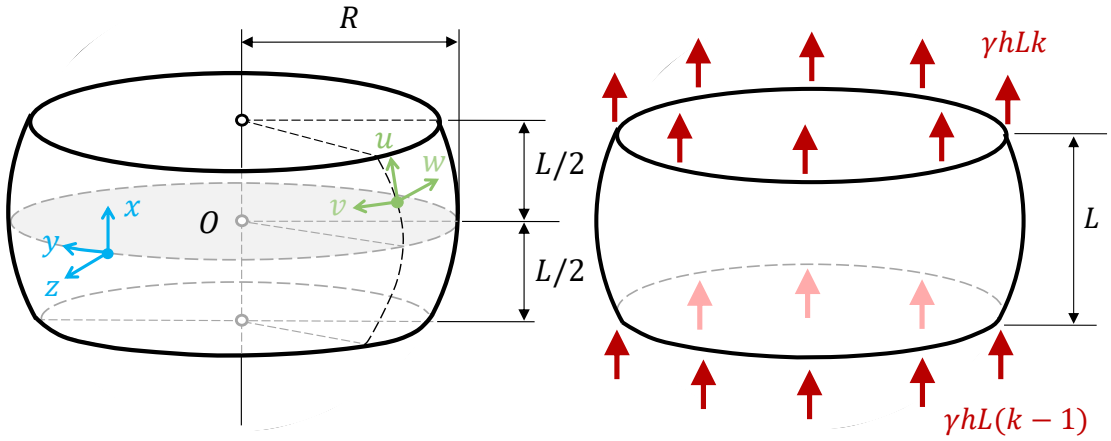

Figure 1: The geometry of the spherical equatorial segment considered in references [23, 24]. Shown in the left diagram are the orientation of the system of coordinates as well as the corresponding displacements; the spherical segment is assumed to be *shallow*, in the sense that $0 < (L/R) \ll 1$. As indicated in the other sketch on the right, this configuration is supported by continuously distributed vertical line reactions at its lower and upper edges; $0 \le k \le 1$ represents the proportion of the total weight supported at the upper edge, while γ is the weight per unit volume of the shell-wall material.

The approach taken by Blum & McComb was purely numerical and relied on formulating this situation as a boundary eigenvalue problem by using simplified shallow-shell theory [1, 17, 25]. The corresponding equations were then solved by using a Galerking-type strategy to identify the critical value, λ_{cr} (say), of a non-dimensional thickness parameter $\lambda \equiv h^2/(12(1-\nu^2)R^2)$; that is, if $\lambda > \lambda_{cr}$ there is no buckling. The numerical results were also compared to a *simplified buckling criterion* stipulating that buckling takes place if the maximum compressive stresses in the equatorial segment exceed the critical compressive stress for a complete sphere loaded by uniform external pressure. The corresponding theoretical critical value for the isotropic state of stress in such a pressurised shell has the well known expression (e.g., [26])

$$\sigma_{cr}^{sph} = \frac{Eh}{R\sqrt{3(1-\nu^2)}}\,. \tag{1.1}$$

Approximations of the foregoing compressive stresses based on linear membrane theory – see equation (2.3) in §2, led Blum & McComb [24] to the upper bound $\lambda_{cr} \leq \lambda_{BM}$, with

$$\lambda_{BM} := \begin{cases} \dfrac{1}{4}(1-k)^2\alpha^2 \equiv \lambda_{BM}^{(-)}\,, & \text{if} \quad 0 \leq k \leq \dfrac{1}{4}\,, \\[2ex] \dfrac{1}{16}(1+2k)^2\alpha^2 \equiv \lambda_{BM}^{(+)}\,, & \text{if} \quad \dfrac{1}{4} \leq k \leq 1\,, \end{cases} \tag{1.2}$$

where $\alpha \equiv \gamma L/E$ and γ represents the specific weight of the material; see Figure 2 for a visual interpretation of formula (1.2). Based on their numerical results they also conjectured that λ_{BM} might in fact be a *least upper bound* for λ_{cr}, but no theoretical arguments were presented in support of this claim. It is one of the main goals of this study to revisit Blum & McComb's mathematical model and provide some theoretical arguments that lend credibility to their conjecture. More specifically, we are going to show that $\lambda_{BM}^{(-)}$ and $\lambda_{BM}^{(+)}$ defined in (1.2) are in fact the leading-order terms in certain asymptotic expansions of λ_{cr} (as $\alpha \to 0^+$), in a sense that will be made clear in §3.

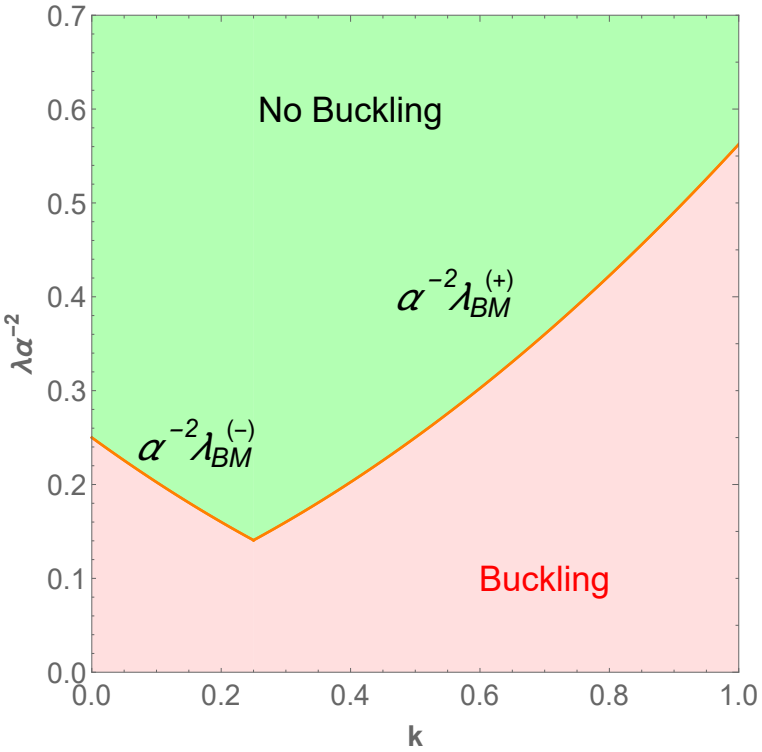

Figure 2: Graphical illustration and interpretation of the upper bound (1.2).

The paper is organised as follows. The coming section contains a brief outline of the main features of the mathematical model that forms the core of this study. By coupling the Donnell-Mushtari-Vlasov (DMV) shallow-shell theory with a suitably determined membrane state of deformation (due to the shell's own weight) results in a boundary eigenvalue value problem that is eventually reduced to a single fourth-order differential equation with variable coefficients and several non-dimensional parameters. We start in §3 with a summary of a numerical investigation of this equation that complements the earlier results published in [23, 24]. In particular, we focus on the localisation of the eigenmodes near the shell's edges by delineating two main such regimes of interest. The insight gained from

this preliminary numerical study proves instrumental in guiding us through the asymptotic work that takes up the rest of the paper. Based on the asymptotic strategy developed in some of our previous studies [27, 28, 29, 30], in §4 we propose a boundary-layer type approximation for the case when the eigenmodes are localised near the upper rim of the shell; such axially localised deformations are also characterised by a regular short-wavelength rippling pattern circumferentially, the number of such ripples being part of the solution as well. The localisation near the lower edge of the shell is more tricky to capture because it consists of a fast spatial oscillation modulated on a large scale by a boundary-layer type envelope. We show in §5 that the naive extension of the approach followed in §4 does not lead to approximations for the critical load λ_{cr}. To address this apparent shortcoming, an ad-hoc WKB-type approach for a fourth-order differential equation is suggested in §6. The paper concludes in §7 with a brief discussion of the main results and their implications.

2 Formulation

To make the paper reasonably self-contained, in this section we include an outline of the relevant equations describing the buckling of the configuration shown in Figure 1. As already discussed in §1, our main interest lies in the possible instabilities of that spherical equatorial segment due to its own weight and the way it is supported along its circular boundaries. The former aspect requires taking into account the body forces, $\boldsymbol{p}$ (say), in the corresponding shell equations; resolving the weight of the shell in directions tangent (' $\parallel$ ') and normal ('$\perp$') to the shell mid-surface, respectively, we can write

$$\boldsymbol{p} = \boldsymbol{p}_{\parallel} + p_{\perp}\boldsymbol{e}_R \simeq (-\gamma h, 0, 0) - \frac{\gamma h}{R} x \boldsymbol{e}_R \,, \tag{2.1}$$

where $\boldsymbol{e}_R$ is the usual unit radial vector (pointing away from the geometric centre O), and quadratic terms in x have been dropped from the expression recorded in (2.1).

Incorporating the above body-force into the Donnell-Mushtari-Vlasov (DMV) shallow-shell equations (e.g., [1, 25]) leads to

$$\begin{cases} \boldsymbol{\nabla}\cdot\boldsymbol{N} + \boldsymbol{p}_{\parallel} = \boldsymbol{0}\,, & \text{(2.2a)} \\[2ex] \dfrac{Eh^3}{12(1-\nu^2)}\nabla^4 w + \dfrac{1}{R}(N_{xx}+N_{yy}) - \boldsymbol{\nabla}\cdot(\boldsymbol{N}\cdot\boldsymbol{\nabla}w) + p_{\perp} = 0\,, & \text{(2.2b)} \end{cases}$$

where $\boldsymbol{N} = (N_{ab})$ (for $a, b \in \{x, y\}$) represents the usual two-dimensional tensor of membrane stress resultants, the differential operators correspond to

$$\boldsymbol{\nabla} := \left(\frac{\partial}{\partial x}, \frac{\partial}{\partial y}\right), \qquad \nabla^2 := \boldsymbol{\nabla}\cdot\boldsymbol{\nabla} \equiv \frac{\partial^2}{\partial x^2} + \frac{\partial^2}{\partial y^2}\,, \qquad \nabla^4 = \nabla^2\nabla^2\,,$$

and the rest of the notations have the usual meaning (e.g., see [31]).

Buckling equations associated with the DMV system (2.2) are typically obtained by using the *method of adjacent equilibrium* (e.g., see [1, 25]). In principle, this requires finding first the so-called *basic state*; in the present context it corresponds to a particular solution of the system (2.2), in which nonlinearities are discarded and axial symmetry is postulated a priori (i.e., N_{xx}, N_{yy}, w are taken to be independent of y, and $N_{xy} \equiv 0$). Letting $\mathring{\boldsymbol{N}} \equiv \mathring{\boldsymbol{N}}(x)$ be the membrane stress resultants tensor associated with such a basic state, it is a straightforward task to establish that

$$\mathring{N}_{xx} \simeq \gamma h\left[x + \left(k - \frac{1}{2}\right)L\right] \qquad \text{and} \qquad \mathring{N}_{yy} \simeq -\gamma h\left[2x + \left(k - \frac{1}{2}\right)L\right], \tag{2.3}$$

where in these expressions nonlinear contributions in x and terms of order $(L/R)^2$ have been left out; for full details of the derivations, see Appendix B of [24]. Under the usual standard simplifications, the buckling equations that follow by applying the adjacent equilibrium technique can be shown to consist of

$$\begin{cases} \boldsymbol{\nabla}\cdot\boldsymbol{N}=\boldsymbol{0}\,, & \text{(2.4a)} \\ \dfrac{Eh^3}{12(1-\nu^2)}\nabla^4 w+\dfrac{1}{R}(N_{xx}+N_{yy})-\boldsymbol{\nabla}\cdot(\mathring{\boldsymbol{N}}\cdot\boldsymbol{\nabla}w)=0\,, & \text{(2.4b)} \end{cases}$$

where now $\boldsymbol{N}\equiv\boldsymbol{N}(x,y)$ and $w\equiv w(x,y)$ represent the infinitesimal buckling fields. In the present context these equations are amenable to further simplifications as explained next.

By introducing the scalar stress potential $\Phi\equiv\Phi(x,y)$ so that

$$\boldsymbol{N}=(\nabla^2\Phi)\boldsymbol{I}_2-\nabla\otimes\nabla\Phi\,, \tag{2.5}$$

with $\boldsymbol{I}_2$ being the two-dimensional identity tensor and $\boldsymbol{\nabla}\otimes\boldsymbol{\nabla}\Phi$ the Hessian of the stress function, the vector equation (2.4a) turns out to be identically satisfied (e.g., see [31], pp. 379-380), while the system (2.4) is replaced by (2.4b) together with the (scalar) compatibility relation

$$\nabla^4\Phi=\left(\frac{Eh}{R^2}\right)\nabla^2 w\,. \tag{2.6}$$

We note that by expanding the divergence term in (2.4b) and using (2.2a) we are led to the equivalent form

$$\frac{Eh^3}{12(1-\nu^2)}\nabla^4 w+\underline{\frac{1}{R}(N_{xx}+N_{yy})}+\boldsymbol{p}_{\parallel}\cdot(\boldsymbol{\nabla}w)-\mathring{\boldsymbol{N}}:\big(\boldsymbol{\nabla}\otimes\boldsymbol{\nabla}w\big)=0\,; \tag{2.7}$$

in this equation the 'colon' stands for the (vertical) double-contracted product (if $\boldsymbol{T}$, $\boldsymbol{S}$ are two second-order Cartesian tensors then $\boldsymbol{T}:\boldsymbol{S}\equiv T_{ab}S_{ab}$, where repeated indices are implicitly summed over). In light of (2.5), the underlined term in equation (2.7) can be replaced by $R^{-1}\nabla^2\Phi$, so that the buckling system turns out to involve two coupled fourth-order partial differential equations for the transverse displacement w and the stress potential Φ. However, as shown in [23, 24], for simply-supported edge conditions the equation (2.7) can be cast entirely in terms of w. More specifically, the boundary conditions adopted in that work correspond to

$$N_{xx}=0\,,\qquad v=0\,,\qquad w=0\,,\qquad \frac{\partial^2 w}{\partial x^2}=0\,,\qquad \text{for } x=\pm\frac{L}{2}\,. \tag{2.8}$$

When the above observation regarding the underlined term in (2.7) is used in conjunction with equations (2.6) and (2.8), it transpires that $R^{-1}\nabla^2\Phi=(Eh/R^2)w$, and then (2.7) can be finally stated as

$$\frac{Eh^3}{12(1-\nu^2)}\nabla^4 w+\left(\frac{Eh}{R^2}\right)w+\boldsymbol{p}_{\parallel}\cdot(\boldsymbol{\nabla}w)-\mathring{\boldsymbol{N}}:\big(\boldsymbol{\nabla}\otimes\boldsymbol{\nabla}w\big)=0\,. \tag{2.9}$$

The upshot here is that we have an equation that depends solely on the transverse displacement; we still have to solve (2.6) in order to be able to enforce all the boundary conditions (2.8), but the two main equations are decoupled (and the same is true of the boundary constraints). To summarise, the starting point of all the developments included in the remaining of this paper is the simplified DMV buckling system consisting of equations (2.6) and (2.9) subject to the boundary constraints (2.8). The

solution strategy for this buckling problem is based on the standard *normal-mode approach* as outlined next.

The first step is to rescale the equations in order to identify the key non-dimensional parameters which our equations depend on. By introducing the new definitions listed below,

$$\overline{x} := \frac{x}{L}\,, \qquad \overline{y} := \frac{y}{R}\,, \qquad \widehat{w} := \frac{w}{R}\,, \qquad \widehat{\Phi} := \frac{\Phi}{EhR^2}\,, \tag{2.10a}$$

$$\lambda := \frac{h^2}{12(1-\nu^2)R^2}\,, \qquad \alpha := \frac{\gamma L}{E}\,, \qquad \beta := \frac{R}{L}\,, \tag{2.10b}$$

routine algebraic manipulations lead to

$$\begin{cases} \lambda\nabla_*^4\widehat{w} + \widehat{w} - \alpha\beta^2\dfrac{\partial\widehat{w}}{\partial\overline{x}} - \alpha\beta^2 f(\overline{x};k)\dfrac{\partial^2\widehat{w}}{\partial\overline{x}^2} + \alpha g(\overline{x};k)\dfrac{\partial^2\widehat{w}}{\partial\overline{y}^2} = 0\,, & \text{(2.11a)} \\[2ex] \nabla_*^4\widehat{\Phi} = \nabla_*^2\widehat{w}\,, & \text{(2.11b)} \end{cases}$$

where

$$\nabla_*^2 := \beta^2\frac{\partial^2}{\partial\overline{x}^2} + \frac{\partial^2}{\partial\overline{y}^2}\,, \qquad \nabla_*^4 := \beta^4\frac{\partial^4}{\partial\overline{x}^4} + 2\beta^2\frac{\partial^4}{\partial\overline{x}^2\partial\overline{y}^2} + \frac{\partial^4}{\partial\overline{y}^4}\,,$$

and

$$f(\overline{x};k) := \overline{x} + \left(k - \frac{1}{2}\right)\,, \qquad g(\overline{x};k) := \overline{x} + f(\overline{x};k)\,.$$

As already noted in the previous section, the non-dimensional thickness λ plays the role of eigenvalue in (2.11), while α, β, and k are parameters that control the mechanical and geometrical characteristics of the configuration considered. It should be clear that the eigenvalue(s) will be function(s) of these quantities, i.e. $\lambda = \lambda(\alpha,\beta,k)$. Furthermore, finding λ involves only the equation (2.11a) subject to appropriate boundary conditions (which will be recorded later on in this section). Once $\widehat{w}$ has been identified, one can use equation (2.11b) to recover $\widehat{\Phi}$, and then the stress distribution in the buckled shell segment follows immediately from a rescaled version of (2.5).

To avoid complicating the notation unnecessarily, in what follows we shall drop the 'bar' on x and y; thus $|x| \le 1/2$ and $y \in [0, 2\pi)$. Solutions with separable variables of the non-dimensional system (2.11) will be sought in the form

$$\widehat{w}(x,y) = W(x)\cos(my)\,, \qquad \widehat{f}(x,y) = F(x)\cos(my)\,, \tag{2.12}$$

with the arbitrary integer $m \ge 0$ being determined subject to the requirement that it should render the global *maximum* of the curve $\lambda = \lambda(m)$ while all the other parameters are kept fixed; the functions W and F replace the original unknowns $\widehat{w}$ and $\widehat{f}$, respectively.

The numerical results reported in [24] revealed that $0 < \alpha \ll 1$ and $\lambda = \mathcal{O}(\alpha^2)$, which suggests writing $\lambda = \lambda_0\alpha^2$, for some $0 < \lambda_0 = \mathcal{O}(1)$. Substituting (2.12) into (2.11), and introducing the additional non-dimensional quantities

$$n := m\beta^{-1}\,, \qquad \mu := \alpha^{-1}\beta^{-2}\,, \qquad \delta := \mu/\lambda_0\,, \tag{2.13}$$

it turns out that the unknown axial amplitudes $W(x)$ and $F(x)$ satisfy a decoupled linear differential system with variable coefficients

$$\left\{(D^2 - n^2)^2 - \delta f(x;k)D^2 - \delta D + \delta[\mu - n^2 g(x;k)]\right\}W(x) = 0\,, \tag{2.14a}$$

$$\beta^{-2}(D^2-n^2)W(x)-(D^2-n^2)^2F(x)=0\,, \tag{2.14b}$$

where $D\equiv d/dx$. Furthermore, the corresponding boundary conditions follow directly from (2.8),

$$W=\frac{d^2W}{dx^2}=0\,, \qquad \text{for} \quad x=\pm\frac{1}{2}\,, \tag{2.15a}$$

$$F=\frac{d^2F}{dx^2}=0\,, \qquad \text{for} \quad x=\pm\frac{1}{2}\,. \tag{2.15b}$$

Before we provide a brief overview of some of the key features of the numerical solutions of the boundary-value problem consisting of (2.14a) and (2.15a), a couple of observations are in order. First, it must be noted that in light of (2.13) the new eigenvalue in this problem is $\delta=\mathcal{O}(\mu)$. Our rescaled version of Blum & McComb's equations [24] is better suited for asymptotic developments, not least because now the critical eigenvalue corresponds to the *positive minimum* of δ as a function of the re-scaled mode number n (treated as a continuous rather than as a discrete quantity). On the other hand, once an asymptotic expansion for δ has been established, one has to invert it because the link with the original λ is essentially through λ_0, which appears in the denominator of the definition for the new eigenvalue – see equation (2.13). The second observation we want to make pertains to the typical orders of magnitude for α defined in (2.10b). As noted in [23, 24], most metalic materials have $\gamma/E=\mathcal{O}(10^{-7})$ (per metre), while for plastics $\gamma/E=\mathcal{O}(10^{-6})$ (per metre), so $\mathcal{O}(10^{-7})\leq\alpha\equiv\gamma L/E\leq\mathcal{O}(10^{-4})$, which ensures that the condition $0<\alpha\ll 1$ is satisfied. It is this particular feature that makes it possible to employ asymptotic methods; in light of definition (2.13) this is also equivalent to $\mu\gg 1$.

Our discussion below establishes the asymptotic structure of the problem considered in this section, and highlights some features that have hitherto not received much attention.

3 Numerical results

The eigenvalues of the boundary-value problem stated at the end of the previous section were first investigated numerically by Blum [23] and Blum & McComb [24]. Taking advantage of the form of the boundary constraints (2.15), they expanded $W(x)$ and $F(x)$ in Fourier sine series, whose unknown coefficients were subsequently computed by applying a Galerkin-type numerical strategy. This leads to a generalised algebraic eigenvalue problem that can be solved by using standard computational algorithms (e.g., see [1, 2]). Unfortunately, the shapes of the eigenmodes were not included in the original studies [23, 24]. It is the purpose of this section to complement the aforementioned earlier works by briefly discussing the nature of the eigenmodes when $\mu\gg 1$. To avoid the numerical difficulties reported by our predecessors, we carried out the computations by using a modified tau spectral method [32] (see also [33, 34]), while the accuracy of the computed eigenvalues was also confirmed by resorting to the compound matrix method (e.g., see [35, 36, 37]).

A rough qualitative understanding of the nature of the shell eigen-deformations can be gleaned from the membrane stress resultants associated with the basic state (2.3). Figure 3 contains a graphical representation of the axial regions that are either in tension or compression as $0\leq k\leq 1$ varies. Strictly speaking, we are only interested in the limiting cases $|k-1|=\mathcal{O}(1)$ (left window) and $|k-1|\ll 1$ (right window); however, for the sake of completeness, we have included plots of $\mathring{N}_{xx}$ and $\mathring{N}_{yy}$ for the entire range of the parameter k. The right window suggests that as $k\simeq 1$, $\mathring{N}_{xx}>0$ for almost all values of x (except, possibly, a small region near the lower rim of the shell); at the same time, $\mathring{N}_{yy}<0$ for $-0.25\lesssim x\leq 0.5$, i.e. we have azimuthal compression in this region, and we note further that its maximum absolute value is at $x=0.5$. We are going to see shortly that for $k\simeq 1$ the buckling

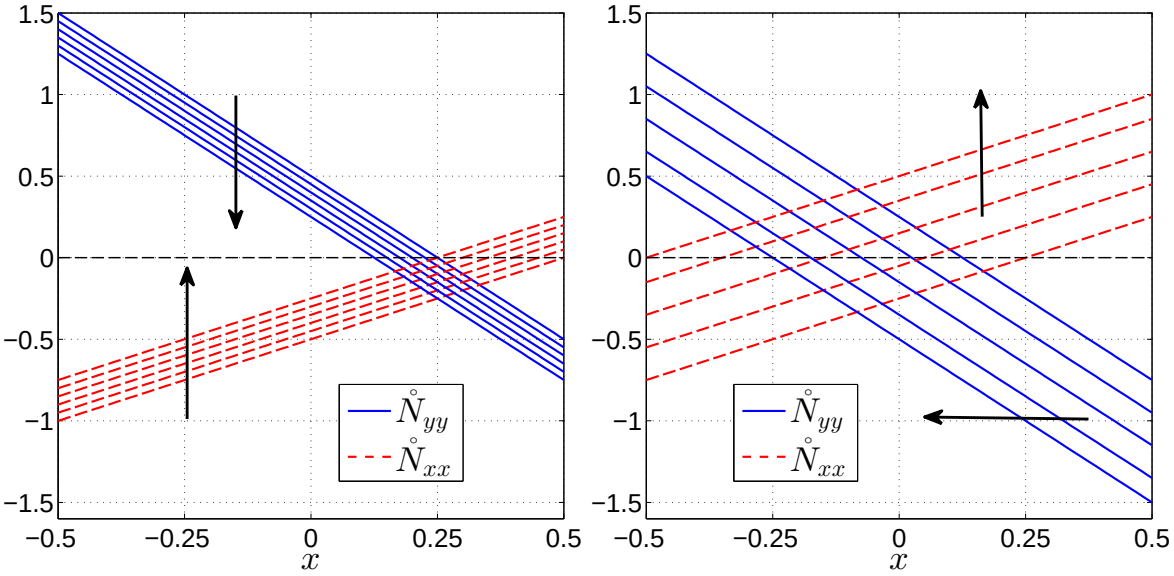

Figure 3: The dependence of the (non-dimensionalised) pre-buckling membrane stresses (2.3) on $0 \leq k \leq 1$: $k = 0.0, 0.05, 0.1, 0.15, 0.2, 0.25$ (left), and $k = 0.25, 0.45, 0.65, 0.85, 1.0$ (right). In both windows the arrows show the direction in which k increases; $\mathring{N}_{xx}$ and $\mathring{N}_{yy}$ have been normalised by taking $\gamma h = 1$.

pattern is axially localised near the upper rim of the shell and is also characterised by a regular short-wavelength deformation pattern circumferentially. The left window of Figure 3 sheds some light on the case $k \simeq 0$. In particular, $\mathring{N}_{xx} < 0$, except (possibly) near $x = 0.5$, and its maximum absolute value is at $x = -0.5$ (lower rim of the shell). We can also see that $\mathring{N}_{yy} > 0$, at least for $-0.5 \leq x \lesssim 0.25$, so it is likely that the buckling will have an axisymmetric character. Again, we will confirm shortly that in this case the buckling is indeed purely axial and is confined near the lower rim. It also turns out that, in contrast to the other scenario, this local buckling pattern has a richer spatial structure as explained next.

The *axisymmetric* nature of the buckling deformations for the case $|k - 1| = \mathcal{O}(1)$ is confirmed by the monotonic increasing behaviour of the response curves $\delta = \delta(n)$ included in the left window of Figure 4; clearly, all the curves shown have a global minimum at $n = 0$. In the right window of the same Figure, we kept k fixed (either 10^{-1} or 10^{-2}, respectively) and varied β for a sample of illustrative values. The conclusion that transpires from the numerical evidence included therein is that, for a fixed β, the response curve $\delta = \delta(n)$ is shifted down as k decreases. In both windows of Figure 4 we have used $\alpha = 10^{-5}$ but the same behaviour persists for other smaller values that we have tested (e.g., 10^{-6} and 10^{-7}).

Examples of typical axisymmetric modes for the case $0 < k < 1/4$ are included in Figures 5 and 6 – we refer to the corresponding captions for the specific values of the parameters used in the numerical simulations. For reasons that will become apparent later on (in §6), we show the eigenmodes associated with the smallest and second smallest positive eigenvalues δ. Both sets of functions have a similar structure consisting of a modulated spatial oscillation. The *critical* modes are those in the left windows ('critical' in the sense that the eigenvalues associated with them are less than those corresponding to the functions recorded in the right window). We shall refer to these latter functions as the *shadowing*

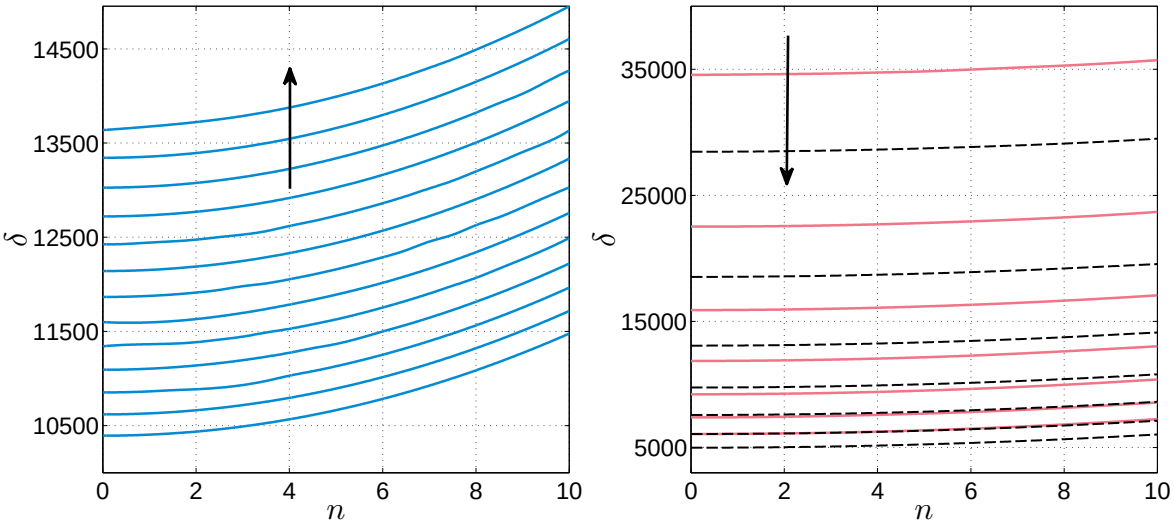

Figure 4: Sample of response curves $\delta = \delta(n)$ for the case $0 < k < 1/4$; in both sets of plots $\alpha = 10^{-5}$. However, on the left, $\beta = 7$ and each curve corresponds to $k = j \times 10^{-2}$ with $j = 4, 5, \ldots, 15, 16$ (the arrow indicates the direction in which k increases). On the right, $k = 0.1$ (solid lines) or $k = 0.01$ (dashed lines), while $\beta = 4, 5, \ldots, 9, 10$ (the arrow indicates the direction in which this latter parameter increases).

eigenmodes because the eigenvalues λ for both sets of functions satisfy

$$\lim_{\alpha \to 0^+} \left(\frac{\lambda}{\alpha^2} \right) = \frac{1}{4}(1-k)^2 \, .$$

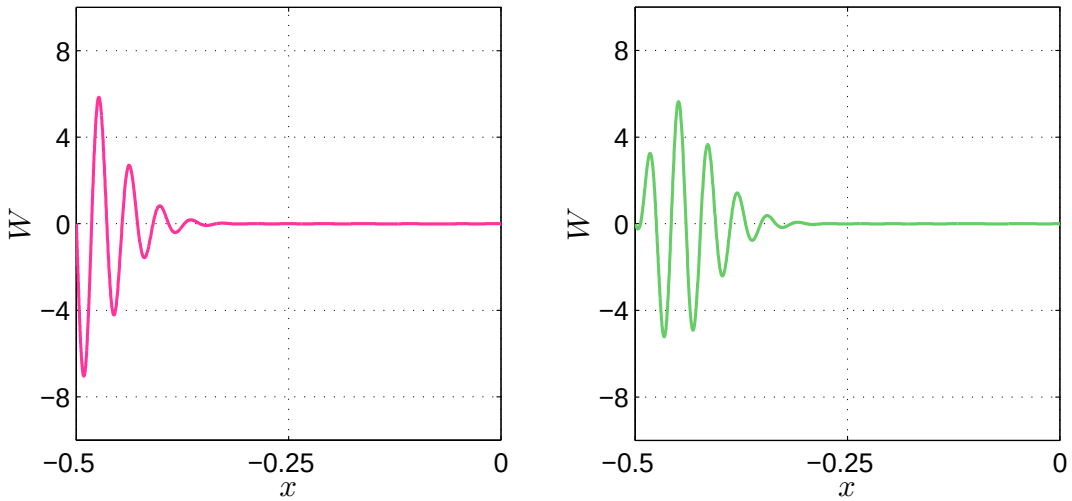

Figure 5: The first two (axisymmetric) modes of the boundar-value problem consisting of (2.14) subject to the boundary conditions (2.15a), in the case when $0 < k < 1/4$; here, $k = 0.15$, $\beta = 4$, and $\alpha = 5 \times 10^{-6}$. The integration range is restricted to $-1/2 \leq x \leq 0$ since the eigenmodes are localised near the lower rim (i.e., near $x = -1/2$).

Although the above limit is the same for both families of eigenmodes, and the corresponding rates of

convergence are identical, there is an important difference. More precisely, if $\lambda_L^{(I)}$ and $\lambda_L^{(II)}$ denote the eigenvalues corresponding to, respectively, the primary and the shadowing modes mentioned above, we are going to establish that

$$\lambda_L^{(I)} = \lambda_{BM}^{(-)}\left[1 - K_I\alpha^{1/3} + \mathcal{O}(\alpha^{2/3})\right] \quad \text{and} \quad \lambda_L^{(II)} = \lambda_{BM}^{(-)}\left[1 - K_{II}\alpha^{1/3} + \mathcal{O}(\alpha^{2/3})\right] \tag{3.1}$$

as $\alpha \to 0^+$, where the notation $\lambda_{BM}^{(-)}$ was introduced earlier in equation (1.2), and $K_I \neq K_{II} > 0$ are some positive constants.

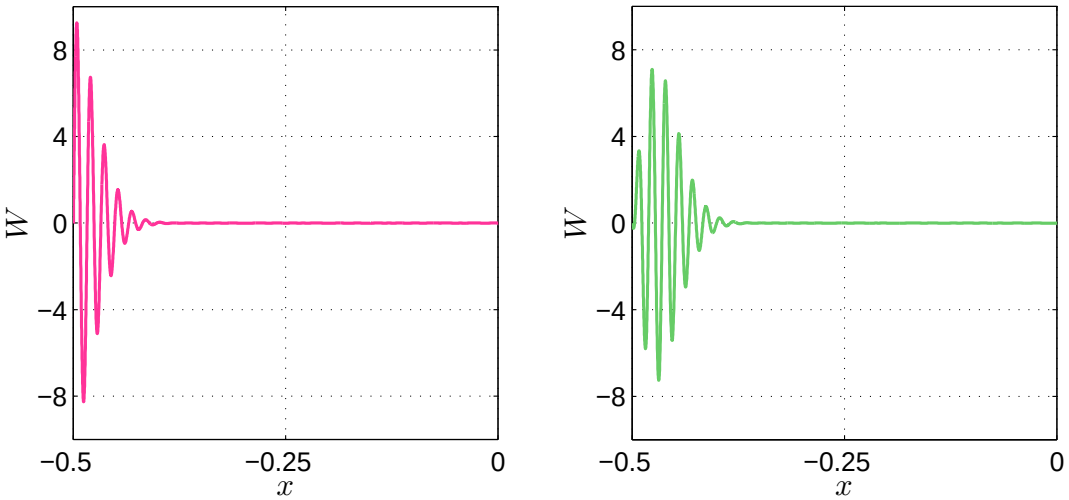

Figure 6: As per Fig. 5, except that here $\alpha = 10^{-6}$.

Turning now to the other case, $|1-k| \ll 1$, the situation is somewhat more straightforward but the buckling modes are *non-symmetric*. To identify the critical mode number we must first find the global minimum of $\delta = \delta(n)$; samples of such curves are illustrated in Figure 7 for two values of $0 < \alpha \ll 1$ while keeping β fixed. The minima of these curves are indicated by circular markers, and we note that as α is decreased from 10^{-5} (left window) to 10^{-7} (right window) there is a sharp increase in the critical mode number. Our extensive numerical simulations suggest that the dependence of this quantity on the asymptotic parameter is $\mathcal{O}(\alpha^{-1/2})$. The two sets of critical eigenmodes associated with the aforementioned white markers are recorded in Figure 8. It is clear that the degree of localisation experienced by these functions is directly linked to the magnitude of α: the smaller this parameter is, the more localised the eigenmodes become – an observation that confirms the boundary-layer nature of the axial deformations and which will play a crucial role in the next section. Furthermore, we are going to show that if λ_R denotes the critical eigenvalue corresponding to such eigenmodes, then

$$\lambda_R = \lambda_{BM}^{(+)}\left[1 - \mathcal{O}(\alpha^{1/3})\right], \qquad \text{as} \quad \alpha \to 0^+, \tag{3.2}$$

where we recall that $\lambda_{BM}^{(+)}$ has already been defined in (1.2).

In the remainder of the paper asymptotic methods will be used to substantiate the numerical findings summarised above. The case of localised deformations near the upper rim of the shell will be discussed first as this has many similarities with some of our previous studies (e.g., [27, 29, 43]).

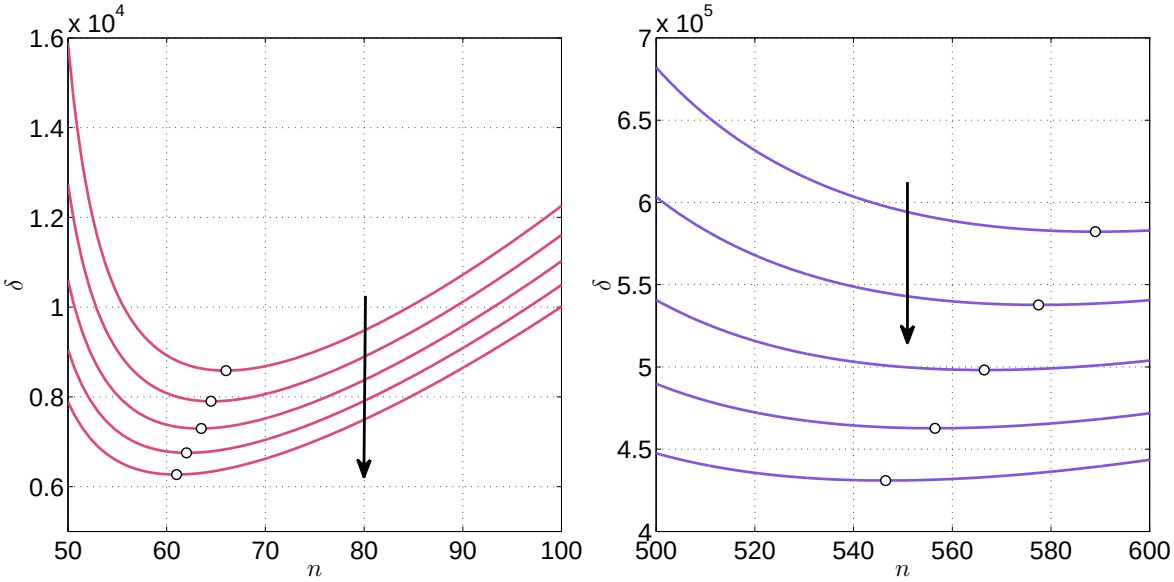

Figure 7: Samples of response curves for the case $1/4 < k < 1$: $\alpha = 10^{-5}$ (left) and $\alpha = 10^{-7}$ (right). In both windows $\beta = 7$ and $k = 0.75, 0.80, 0.85, 0.90, 0.95$ (the arrows show the direction in which this parameter increases). The white markers identify the global minima of the corresponding response curves.

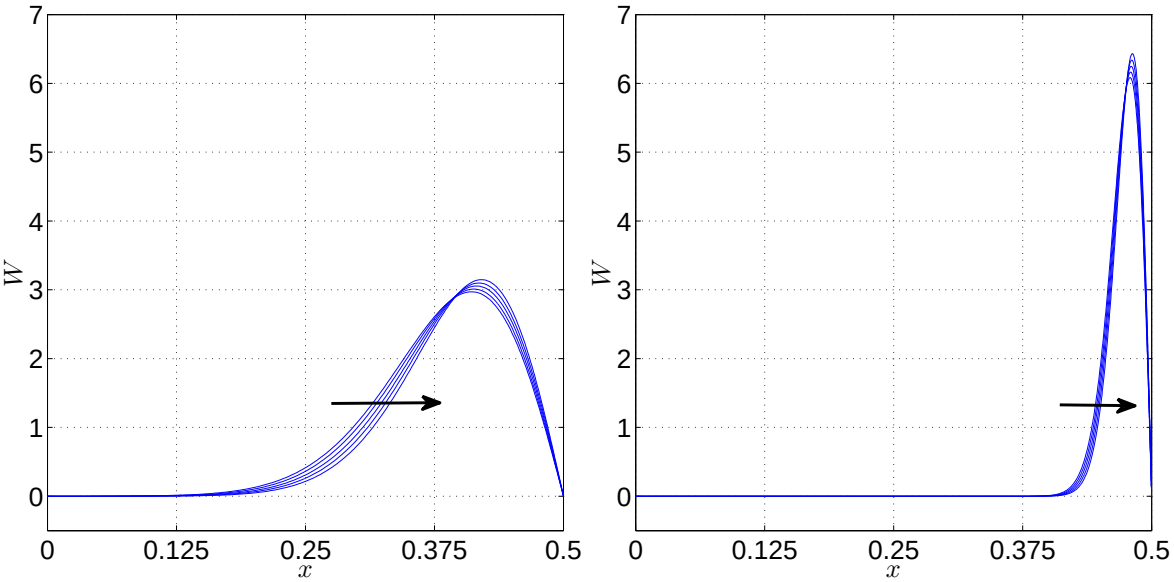

Figure 8: *Critical* eigenmodes associated with the circular white markers in Fig. 7: $\alpha = 10^{-5}$ (left) and $\alpha = 10^{-7}$ (right). The arrows have the same meaning as in the foregoing figure. The range of the independent variable 'x' has been restricted to $0 \leq x \leq 1/2$ since the deformation is localised near the upper rim of the shell (i.e., near $x = 1/2$).

4 The case $1/4 < k < 1$: localisation near the upper rim

The information recorded in Figure 8 anticipates that when $0 \leq |1-k| \ll 1$ the eigenmodes of the bifurcation system (2.14)-(2.15) are confined within a thin layer near $x = 1/2$; also, the mode number seems to increase as $\alpha \to 0^+$ (or, equivalently, as $\mu \to +\infty$). Since we already expect that $\delta = \mathcal{O}(\mu)$, routine scaling arguments indicate that the thickness of the boundary layer is $\mathcal{O}(\mu^{-1/3})$. This suggests the introduction of the re-scaled independent variable $X > 0$ defined by

$$x = \frac{1}{2} - \mu^{-1/3} X \,, \qquad \text{with} \qquad X = \mathcal{O}(1) \,. \tag{4.1}$$

By letting

$$\boldsymbol{u} := \left[\begin{array}{c} W \\ \\ \mu F \end{array} \right] , \qquad \boldsymbol{u}^{(j)}(X) := \left[\begin{array}{c} W_j(X) \\ \\ F_j(X) \end{array} \right] , \qquad (j = 0, 1, 2, \dots) \,,$$

we look for solutions of (2.14) satisfying an ansatz of the form

$$n^2 = N_0 \mu + N_1 \mu^{2/3} + \dots \,, \tag{4.2a}$$

$$\delta = \delta_0 \mu + \delta_1 \mu^{2/3} + \delta_2 \mu^{1/3} + \dots \,, \tag{4.2b}$$

$$\boldsymbol{u}(X) = \boldsymbol{u}^{(0)}(X) + \mu^{-1/3} \boldsymbol{u}^{(1)}(X) + \mu^{-2/3} \boldsymbol{u}^{(2)}(X) + \dots \,. \tag{4.2c}$$

The constants N_j, $\delta_j = \mathcal{O}(1)$ in (4.2a) and (4.2b), as well as the individual terms $\boldsymbol{u}^{(j)}(X)$ on the right-hand side of (4.2c), are found as usual by substituting the assumed form of the solution in the original differential equations, collecting like powers of μ, and then setting to zero the corresponding coefficients. The outcome is a hierarchy of de-coupled equations that are best solved sequentially on a case-by-case basis.

The zeroth-order equations lead to an algebraic relation between δ_0 and N_0,

$$\delta_0 - \frac{1}{2} \delta_0 N_0 - k \delta_0 N_0 + N_0^2 = 0 \,, \tag{4.3}$$

as well as a further algebraic link between F_0 and W_0,

$$F_0 = -\frac{1}{N_0 \beta^2} W_0 \,. \tag{4.4}$$

For the time being we have no use for this latter relation, but it should be clear that once W_0 becomes available, F_0 is fully determined; the boundary conditions on F_0 will be automatically satisfied if W_0 satisfies the constraints (2.15a).

As (4.3) involves two unknown quantities, we solve for δ_0 in terms of N_0,

$$\delta_0 = \frac{2 N_0^2}{(2k+1) N_0 - 2} \,, \tag{4.5}$$

and then look for possible values $N_0 = N_0^*$ (say) for which δ_0 is minimised. Using the criticality condition $\partial \delta_0 / \partial N_0 = 0$ yields

$$N_0^* \equiv 2 \left(k + \frac{1}{2} \right)^{-1} \,, \tag{4.6}$$

so that the corresponding minimum value δ_0 turns out to be

$$\delta_0^* := \delta_0\Big|_{N_0=N_0^*} \equiv 4\left(k+\frac{1}{2}\right)^{-2} . \tag{4.7}$$

We remark in passing that this result ties in with the value of λ_{BM} recorded in equation (1.2). This observation can be easily checked by recalling our definition of δ and μ – see (2.13), as well as Blum & McComb's definition of the eigenvalue λ (which is the same as ours – see (2.10)).

The first-order equation that results from the W-equation in (2.14) assumes the form

$$\omega_1 W_0'' + \omega_2 W_0 = 0\,, \tag{4.8}$$

with

$$\omega_1 := 2N_0 + k\delta_0\,, \tag{4.9a}$$

$$\omega_2 := -\delta_1\left[1-\left(k+\frac{1}{2}\right)N_0\right] - 2\delta_0 N_0 X + N_1\underline{\left[\left(k+\frac{1}{2}\right)\delta_0 - 2N_0\right]}\,; \tag{4.9b}$$

the 'dash' in (4.8) stands for differentiation with respect to X, a convention that will be employed for the rest of this section. When $N = N_0^*$ and $\delta_0 = \delta_0^*$, the underlined term in (4.9b) vanishes, and then (4.8) can be cast as

$$W_0'' - (\Gamma_1 X + \Gamma_2) W_0 = 0\,, \tag{4.10}$$

where

$$\Gamma_1 := \frac{16}{(2k+1)(4k+1)} \qquad \text{and} \qquad \Gamma_2 := -\frac{\delta_1^*(2k+1)^2}{8(4k+1)}\,, \tag{4.11}$$

with

$$\delta_1^* := \delta_1\Big|_{\substack{N_0=N_0^*\\ \delta_0=\delta_0^*}} .$$

Equation (4.10) is amenable to further simplifications by adopting a suitable re-scaling of the independent variable

$$Z := \Gamma_1^{1/3} X + \frac{\Gamma_2}{\Gamma_1^{2/3}}\,, \tag{4.12}$$

whereupon it follows that $d^2\widehat{W}_0/dZ^2 - Z\widehat{W}_0 = 0$, with $\widehat{W}_0(Z) \equiv W_0(X)$. The solution of interest is $\widehat{W}_0 = \mathrm{Ai}(Z)$, where 'Ai' is the usual Airy function that decays exponentially quickly as $Z \to +\infty$.

The boundary conditions (2.15a) at $x = 1/2$ (i.e., at $X = 0$) can both be imposed by requiring that $W_0 \to 0$ as $X \to 0^+$. We recall in passing that, in addition to decaying exponentially as $Z \to +\infty$, the Airy function possesses a countable set of zeros along the negative Z-axis; the first occurs at $(-\zeta_0) \simeq -2.338$, so we can ensure that $W_0(X) = 0$ at $X = 0$ by demanding $\Gamma_1^{-2/3}\Gamma_2 = -\zeta_0$. If the expressions (4.11) are substituted in this relation, it follows immediately that

$$\delta_1^* = 8\zeta_0(4k+1)^{1/3}\left(k+\frac{1}{2}\right)^{-8/3} . \tag{4.13}$$

The first-order equation that follows from the compatibility equation in (2.14) is simply an algebraic link between F_1 and W_0, W_1 (as well as some of their derivatives),

$$F_1 = -(N_0\beta)^{-2}\left[(W_0'' - N_1 W_0) + N_0 W_1\right] . \tag{4.14}$$

Before we can take full advantage of this formula, we need to find N_1 and W_1. This is the next item on our agenda.

The second-order equation that follows from the W-equation in (2.14) is of the form

$$\omega_1 W_1'' + \omega_2 W_1 + \sum_{k,j} c_{kj} X^k \frac{d^j W_0}{dX^j} = 0\,, \tag{4.15}$$

where ω_i $(i = 1, 2)$ have already been defined in (4.9), and the numerous $c_{kj} \in \mathbb{R}$ are complicated constants which can be expressed in terms of the quantities introduced at previous orders. Rather than give the full form of these constants, we remark that (4.15) can be transformed into an inhomogeneous Airy-type equation that is readily solved in closed form. With the aid of the change of variable (4.12), we eventually find

$$\frac{d^2\widehat{W}_1}{dZ^2} - Z\widehat{W}_1 = (C_1 + C_2 Z)\widehat{W}_0(Z) + C_3\widehat{W}_0^{(1)}(Z) + (C_4 + C_5 Z)\widehat{W}_0^{(2)}(Z) + C_6\widehat{W}_0^{(4)}(Z)\,, \tag{4.16}$$

where the subscripts on $\widehat{W}_0$ indicate differentiation with respect to Z and the rather intricate expressions of the coefficients C_j $(j = 1, 2, \ldots, 6)$ are relegated to Appendix A.

Next, we note that a particular solution of (4.16) is given by

$$\widehat{W}_1(Z) = C_1\widehat{W}_0^{(1)}(Z) + \left(\frac{1}{2}C_3 - C_5\right)\widehat{W}_0^{(2)}(Z) + \frac{1}{3}(C_2 + C_4)\widehat{W}_0^{(3)}(Z) + \frac{1}{5}(C_5 + C_6)\widehat{W}_0^{(5)}(Z)\,.$$

To enforce the boundary conditions (2.15a), we need the value of this function as $Z \to (-\zeta_0)$, and it is a simple exercise to check that

$$\widehat{W}_1\Big|_{Z=-\zeta_0} = \left[C_1 - \frac{1}{3}(C_2 + C_4)\zeta_0 + \frac{1}{5}(C_5 + C_6)\zeta_0^2\right]\widehat{W}_0^{(1)}(-\zeta_0)\,. \tag{4.17}$$

By using the definitions of the coefficients C_j from Appendix A, the expression in (4.17) can be re-arranged as a quadratic of N_1, in particular,

$$\widehat{W}_1\Big|_{Z=-\zeta_0} \propto (N_1^2 + q_1 N_1 + q_0)\mathrm{Ai}_0'\,, \qquad \mathrm{Ai}_0' \equiv \mathrm{Ai}'(-\zeta_0)\,, \tag{4.18}$$

in which

$$q_1 := -\frac{4\zeta_0}{3}(14k + 3)(4k + 1)^{-2/3}\left(k + \frac{1}{2}\right)^{-5/3}\,,$$

$$q_0 := -\delta_2 + \frac{4\zeta_0^2}{15}(796k^2 + 360k + 41)(4k + 1)^{-4/3}\left(k + \frac{1}{2}\right)^{-10/3}\,,$$

and the proportionality factor in (4.18) is different from zero. Clearly, for W_1 (and its second-order derivative) to vanish when $X = 0$, we need the first term on the right-hand side in (4.18) to be zero. This provides us with a quadratic of the form $\delta_2 \equiv \delta_2(N_1)$. Minimizing with respect to N_1 yields the stationary point $N = N_1^*$, with

$$N_1^* := \frac{2\zeta_0}{3}(14k + 3)(4k + 1)^{-2/3}\left(k + \frac{1}{2}\right)^{-5/3}\,, \tag{4.19}$$

whereupon

$$\delta_2^* \equiv \delta_2(N_1^*) = \frac{8\zeta_0^2}{45}(704k^2+330k+39)(4k+1)^{-4/3}\left(k+\frac{1}{2}\right)^{-10/3}. \tag{4.20}$$

To summarise, we have identified the terms $\delta_j = \delta_j^*$ $(j=0,1,2)$ corresponding to the *critical* value of the eigenvalue δ in the expansion (4.2b). Taking into account that $\lambda = \lambda_0\alpha^2$ and $\delta = \mu/\lambda_0$ – see (2.13), we can invert (4.2b) to obtain an expansion for the original eigenvalue λ used in [23, 24]. Thus, with the help of (4.7), (4.13), and (4.20) we eventually arrive at the following asymptotic formula

$$\lambda_{cr} = \underline{\frac{1}{16}(2k+1)^2\alpha^2}\left\{1 - 2\sqrt[3]{4}\zeta_0\beta^{2/3}\left[\frac{4k+1}{(8k^2+6k+1)^{2/3}}\right]\alpha^{1/3}\right.$$
$$\left. + \frac{4\sqrt[3]{2}\zeta_0^2}{45}\beta^{4/3}\left[\frac{736k^2+390k+51}{(8k^2+6k+1)^{4/3}}\right]\alpha^{2/3} + \ldots\right\}, \qquad \text{as} \quad \alpha \to 0^+. \tag{4.21}$$

Note that the underlined term in this result is just $\lambda_{BM}^{(+)}$ defined in the Introduction – see (1.2). Finally, the accuracy of the above final result is illustrated in Figure 9 where the predictions of (4.21) are compared against the direct numerical simulations of the original boundary-value problem outlined in §2. For $\beta = 7$ and $\alpha = 10^{-5}$ the relative errors between the two sets of data are between 0.8% and 1.1%, while for $\beta = 4$ and $\alpha = 10^{-7}$ the same errors are typically $\mathcal{O}(10^{-4})$. We also remark that for each value of α tested, the relative errors tend to increase slightly as k decreases away from $k = 1$.

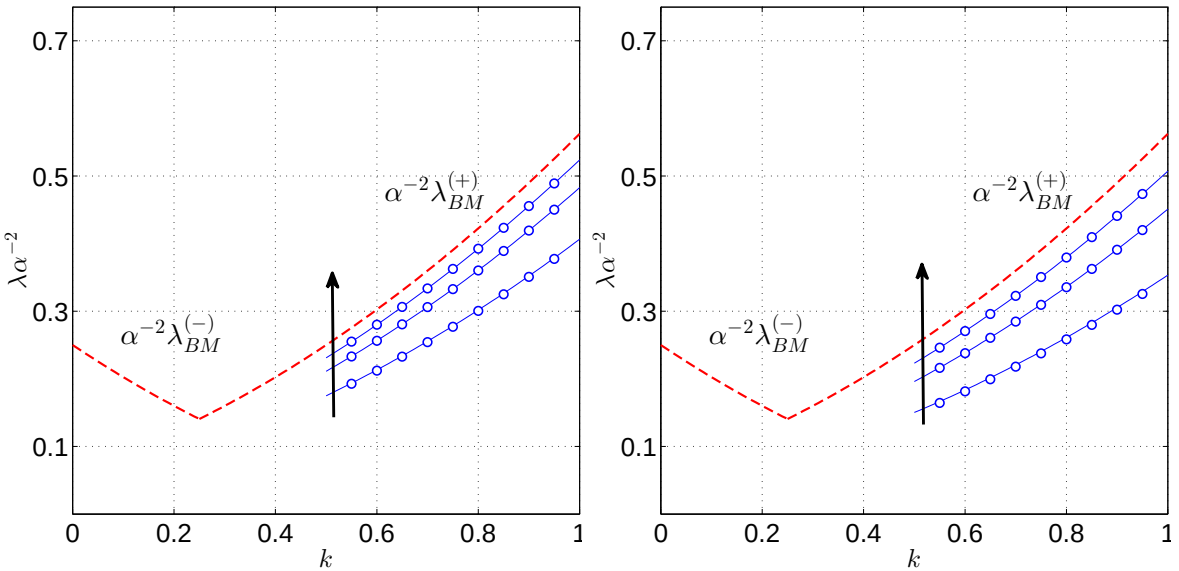

Figure 9: Comparisons of the asymptotic formula (4.21) and direct numerical simulations of the original boundary-value problem (2.14)-(2.15) for $\beta = 4$ (left) and $\beta = 7$ (right). The (red) dashed curve corresponds to the piecewise function (1.2) and represents the *least upper bound* for the eigenvalues λ. In each window, three different values of α have been considered: 10^{-5}, 10^{-6}, and 10^{-7} (the arrows point in the direction in which this parameter decreases). The asymptotic results are indicated by the continuous (blue) curves, while the numerical results correspond to the circular (white) markers.

5 The case $0 < k < 1/4$: a standard approach

As already discovered in §3 (see Figures 5 and 6), when $0 < k < 1/4$ the first two eigenmodes associated with $\delta > 0$ both adopt a multi-scale localised structure in which a spatial oscillation is modulated over a relatively small region adjacent to the lower rim of the shell ($x = -1/2$). Furthermore, the size of this regions shrinks as $\alpha \to 0^+$ (or, equivalently, as $\mu \to +\infty$). Standard scaling arguments can help establish the relevant orders of magnitude of these length-scales, but in the interest of brevity such heuristic arguments will not be re-iterated here. We remark in passing that the structure of the eigenmodes is very similar to the situation encountered in our earlier works regarding the wrinkling of flat annular plates [29, 38, 39] as well as in the recent paper [40] dealing with the azimuthal shearing of a truncated hemispherical elastic shell. With this in mind, we introduce the re-scaled variable $Y > 0$ defined by

$$x = -\frac{1}{2} + \mu^{-1/3} Y \,, \qquad \text{with} \qquad Y = \mathcal{O}(1) \,. \tag{5.1}$$

To avoid running out of symbols for our variables we will recycle some of the previous notations; as each section is self-contained, no confusion should arise.

By letting

$$\boldsymbol{u} := \begin{bmatrix} W \\ \mu F \end{bmatrix} , \qquad \boldsymbol{v}^{(j)}(Y) := \begin{bmatrix} W_j(Y) \\ F_j(Y) \end{bmatrix} , \qquad (j = 0, 1, 2, \dots) \,,$$

we look for solutions of (2.14) satisfying an ansatz of the form

$$\boldsymbol{u} = \boldsymbol{v}(Y) \exp\left(\mathrm{i}\Omega \mu^{1/6} Y\right) , \qquad (\mathrm{i} = \sqrt{-1}) \,, \tag{5.2}$$

where

$$\delta = \delta_0 \mu + \delta_1 \mu^{2/3} + \delta_2 \mu^{1/2} + \delta_3 \mu^{1/3} + \dots \,, \qquad (\delta_j \in \mathbb{R} \,,\ j = 0, 1, 2, \dots) \,, \tag{5.3a}$$

$$\boldsymbol{v}(Y) = \boldsymbol{v}^{(0)}(Y) + \mu^{-1/6} \boldsymbol{v}^{(1)}(Y) + \mu^{-1/3} \boldsymbol{v}^{(2)}(Y) + \mu^{-1/2} \boldsymbol{v}^{(3)}(Y) + \mu^{-2/3} \boldsymbol{v}^{(4)}(Y) + \dots \,; \tag{5.3b}$$

the constant $\Omega \in \mathbb{R}$ is unknown at this stage but will be found as part of the solution (e.g., see [30, 38]). The complex exponential term in (5.2) accounts for the spatial oscillations of the eigenmodes seen in Figures 5 and 6 – these oscillations take place on a $\mathcal{O}(\mu^{-1/2})$ scale which is much shorter than that described by the re-scaled independent variable Y in (5.1). It should be clear the aforementioned ansatz is equivalent to the application of the method of multiple scales (e.g., [41, 42, 43, 44]); this would correspond to introducing the spatial scales $X_1 \equiv \mu^{1/3}(x + 1/2)$ and $X_2 \equiv \mu^{1/2}(x + 1/2)$, and then regarding the dependent variables as functions of both (i.e., $W \equiv W(X_1, X_2)$, $F = F(X_1, X_2)$). However, past experience shows that the final results remain the same, so we shall follow the shorter route outlined above.

The various coefficients $\delta_j = \mathcal{O}(1)$ in the expansion (5.3a) of the eigenvalue δ will be found as in the last section, solving the various reduced equations obtained by substituting (5.2)-(5.3) in the original differential equations.

The zeroth-order equation amounts to the "dispersion" relation

$$\Omega^4 - \delta_0 \Omega^2 (1 - k) + \delta_0 = 0 \qquad \Longrightarrow \qquad \delta_0 = \frac{\Omega^4}{\Omega^2 (1 - k) - 1} \,.$$

It is clear that $\delta_0 \equiv \delta_0(\Omega^2)$ and, as we are looking for the lowest $\delta_0 > 0$, we must search for the critical value(s) of Ω^2 by enforcing the usual stationarity condition $\partial\delta_0/\partial(\Omega^2) = 0$. This equation yields the value $\Omega = \Omega_* > 0$,

$$\Omega_* := \sqrt{2}(1-k)^{-1/2} \qquad \Longrightarrow \qquad \delta_0^* := \delta_0\Big|_{\Omega=\Omega_*} = 4(1-k)^{-2}\,. \tag{5.4}$$

At first-order we find an algebraic relation relating W_1 and the first-order derivative of W_0, which turns out to be identically satisfied when Ω and δ_0 assume the values found in (5.4).

The next non-trivial piece of information emerges at the second-order in the form of

$$\widetilde{\omega}_1 W_0'' + \widetilde{\omega}_2 W_0 + \widetilde{\omega}_3 W_1' + \widetilde{\omega}_4 W_2 = 0\,, \tag{5.5}$$

with

$$\widetilde{\omega}_1 := -6\Omega^2 + \delta_0(1-k)\,, \qquad \widetilde{\omega}_2 := \delta_1\left[1-\Omega^2(1-k)\right] + \Omega^2\delta_0 Y\,, \tag{5.6a}$$

$$\widetilde{\omega}_3 := -2\mathrm{i}\Omega\left[2\Omega^2 - \delta_0(1-k)\right]\,, \qquad \widetilde{\omega}_4 := \Omega^4 - \delta_0[\Omega^2(1-k)-1]; \tag{5.6b}$$

the 'dash' in (5.5) stands for differentiation with respect to Y, a convention that will be employed for the rest of this section. Note that $\widetilde{\omega}_3 = \widetilde{\omega}_4 = 0$ when $\Omega = \Omega^*$ and $\delta_0 = \delta_0^*$, so that (5.5) can be stated in the simplified form

$$W_0'' - (\widetilde{\Gamma}_1 Y + \widetilde{\Gamma}_2) W_0 = 0\,, \tag{5.7}$$

where

$$\widetilde{\Gamma}_1 := (1-k)^{-2} \qquad \text{and} \qquad \widetilde{\Gamma}_2 := -\frac{1}{8}\delta_1^*(1-k)\,, \tag{5.8}$$

with

$$\delta_1^* := \delta_1\Big|_{\substack{\Omega_0=\Omega_0^*\\ \delta_0=\delta_0^*}}\,. \tag{5.9}$$

As in the previous section, all coefficients δ_j $(j = 1, 2, \dots)$ in (5.3a) which are obtained by replacing Ω and δ_0 with their corresponding values recorded in (5.4) will be marked with an asterisk as in (5.9).

Equation (5.7) is just a re-scaled Airy equation that can be cast into the standard form as already discussed in §4. Letting $Z := \widetilde{\Gamma}_1^{1/3} Y + \widetilde{\Gamma}_2 \widetilde{\Gamma}_1^{-2/3}$, (5.7) becomes $d^2\widehat{W}_0/dZ^2 - Z\widehat{W}_0 = 0$, with $\widehat{W}_0(Z) \equiv W_0(Y)$. The solution of interest is $\widehat{W}_0 = \mathrm{Ai}(Z)$, and imposing the requirement that $W_0(Y) = 0$ at $Y = 0$ eventually leads to

$$\delta_1^* = 8\zeta_0(1-k)^{-7/3}\,. \tag{5.10}$$

At the next order the calculations throw an inhomogeneous version of the differential equation (5.7) in which $W_0(Y)$ is replaced by $W_1(Y)$. Changing the independent variable to Z in this new equation yields

$$\frac{d^2\widehat{W}_1}{dZ^2} - Z\widehat{W}_1 = b_1\widehat{W}_0(Z) + (b_2 + b_3 Z)\widehat{W}_0^{(1)} + b_4\widehat{W}_0^{(3)}\,, \tag{5.11}$$

where

$$b_1 := -\frac{\mathrm{i}\sigma}{\sqrt{2}} - \frac{1}{8}\delta_2^*\sigma^{-14}\,, \quad b_2 := \mathrm{i}\zeta_0\sqrt{2}\sigma\,, \quad b_3 := -\mathrm{i}\sqrt{2}\sigma\,, \quad b_4 := \frac{\mathrm{i}\sigma}{\sqrt{2}}\,,$$

and

$$\sigma := (1-k)^{-1/6}\,;$$

the superscript on $\widehat{W}_0$ indicates differentiation with respect to Z. A particular solution of (5.11) is readily identified as

$$\widehat{W}_1(Z) = (b_1 - b_3)\widehat{W}_0^{(1)}(Z) + \frac{1}{2}b_2\widehat{W}_0^{(2)}(Z) + \frac{1}{4}(b_3 + b_4)\widehat{W}_0^{(4)}(Z)\,. \tag{5.12}$$

Recalling that the contribution of $\widehat{W}_1$ to the asymptotic approximation of the eigenmodes is in fact obtained by taking the real part of the product between (5.12) and the complex exponential in (5.2), the satisfaction of the boundary condition $W_1(Y) = 0$ for $Y = 0$ requires that the underlined term in b_1 must vanish; hence $\delta_2^* = 0$.

The next-order equation is again an inhomogeneous Airy-type equation for $W_2(Y)$. Changing the independent variable to Z we obtain

$$\frac{d^2\widehat{W}_2}{dZ^2} - Z\widehat{W}_2 = (c_1 + c_2 Z)\widehat{W}_0(Z) + c_3\widehat{W}_0^{(1)}(Z) + (c_4 + c_5 Z)\widehat{W}_0^{(2)}(Z) + c_6\widehat{W}_0^{(4)}(Z)$$
$$+ c_7\widehat{W}_1(Z) + (c_8 + c_9 Z)\widehat{W}_1^{(1)}(Z) + c_{10}\widehat{W}_1^{(3)}(Z)\,, \tag{5.13}$$

where

$$c_1 := -\frac{1}{8}\delta_3^*\sigma^{-14} + 2(\zeta_0\sigma)^2\,, \quad c_2 := 2\zeta_0\sigma^2\,, \quad c_3 := -\frac{\sigma^2}{2}\,, \quad c_4 := \frac{\zeta_0\sigma^2}{2}\,, \quad c_5 := -\frac{\sigma^2}{2}\,,$$

$$c_6 := \frac{\sigma^2}{8}\,, \quad c_7 := -\frac{\mathrm{i}\sigma}{\sqrt{2}}\,, \qquad c_8 := \mathrm{i}\zeta_0\sqrt{2}\sigma\,, \quad c_9 := -\mathrm{i}\sqrt{2}\sigma\,, \quad c_{10} := \frac{\mathrm{i}\sigma}{\sqrt{2}}\,.$$

The right-hand side of the differential equation (5.13), RHS (say), can be expressed in terms of the Airy function $\mathrm{Ai}(Z)$ and its first derivative, $\mathrm{Ai}'(Z)$, by using (5.12) and standard properties of the Airy equation. After considerable (routine) algebraic manipulations one finds

$$RHS = (d_{00} + d_{01}Z + d_{02}Z^2)\mathrm{Ai}(Z) + (d_{10} + d_{11}Z + d_{12}Z^2 + d_{13}Z^3)\mathrm{Ai}'(Z)\,, \tag{5.14}$$

where the coefficients d_{ij} in the above expression are recorded in Appendix B. Taking into account that the differential operator in (5.13) is self-adjoint when subjected to the boundary/decay conditions considered here, the usual solvability condition for the inhomogeneous differential equation (5.13) involves multiplying RHS in (5.14) by $\mathrm{Ai}(Z)$, followed by integrating the result between $(-\zeta_0)$ and $+\infty$, and then setting the final expression to zero. This gives

$$d_{00}^{(II)}\delta_3^* = d_{00}^{(I)} + d_{01}\mathcal{J}_1 + d_{02}\mathcal{J}_2 + d_{10}\mathcal{J}_3 + d_{11}\mathcal{J}_4 + d_{12}\mathcal{J}_5 + d_{13}\mathcal{J}_6\,, \tag{5.15}$$

where we have written $d_{00} \equiv d_{00}^{(I)} - \delta_3 d_{00}^{(II)}$ and the expressions of the integrals $\mathcal{J}_k$ $(k = 1, 2, \ldots, 6)$ are again relegated to Appendix B; the quantity δ_3^* represents the value δ_3 in the ansatz (5.3a) corresponding to $\Omega = \Omega_*$, $\delta_0 = \delta_0^*$, and $\delta_1 = \delta_1^*$. Making the appropriate substitutions in (5.15) it transpires that

$$\delta_3^* = \frac{55}{6}\zeta_0^2(1-k)^{-8/3}\,. \tag{5.16}$$

The exact same result can also be obtained by finding a particular solution of (5.13) and then enforcing the boundary condition $\widehat{W}_2 = 0$ for $Y = 0$.

To summarise, our calculations so far have yielded a three-term asymptotic approximation for the eigenvalue δ,

$$\delta = 4(1-k)^{-2}\mu\left[1 + 2\zeta_0(1-k)^{-1/3}\mu^{-1/3} + \frac{55}{24}\zeta_0^2(1-k)^{-2/3}\mu^{-2/3} + \dots\right]. \tag{5.17}$$

As in §4, remembering that $\lambda = \lambda_0\alpha^2$ and $\delta = \mu/\lambda_0$, the expansion in (5.17) can be inverted so that we have $\lambda \equiv \lambda(\alpha)$; more specifically,

$$\lambda_{cr} = \underline{\frac{1}{4}(1-k)^2\alpha^2}\left[1 - 2\beta^{2/3}\zeta_0(1-k)^{-1/3}\alpha^{1/3} + \frac{41}{24}\beta^{4/3}\zeta_0^2(1-k)^{-2/3}\alpha^{2/3} + \dots\right], \tag{5.18}$$

and we recall that the underlined term is actually $\lambda_{BM}^{(-)}$ defined in (1.2).

In Table 1 we compare the predictions of (5.18) with the largest and second largest eigenvalues of the original boundary-value problem, which are identified as $\lambda_{cr}^{(1)}$ and $\lambda_{cr}^{(2)}$, respectively. A quick glance at the values included in the last three columns of the aforementioned table reveals that the asymptotic approximation matches closely the second largest eigenvalue $\lambda_{cr}^{(2)}$. The corresponding relative errors are below 1% for all values of $0 < k < 0.25$ considered, whereas the same relative errors for $\lambda_{cr}^{(1)}$ are around 8%. These findings remain valid for larger values α as well as different choices of β.

Table 1: Comparison between the asymptotic result (5.18) and the full numerical simulations of the original boundary-value problem defined in §2; for the latter we have included the largest and second largest eigenvalues, denoted by $\lambda_{cr}^{(1)}$ and $\lambda_{cr}^{(2)}$, respectively. Here, $\beta = 7$ and $\alpha = 5 \times 10^{-7}$.

k	$\alpha^{-2}\lambda_{cr}$ (asymptotics)	$\alpha^{-2}\lambda_{cr}^{(1)}$ (full numerics)	$\alpha^{-2}\lambda_{cr}^{(2)}$ (full numerics)
0.01	0.213580	0.231080	0.214140
0.05	0.196293	0.212540	0.196824
0.10	0.175727	0.190539	0.176215
0.15	0.156314	0.169830	0.156761
0.20	0.138056	0.150183	0.138470

6 The case $0 < k < 1/4$: simplified WKB analysis

We re-consider the case discussed in the previous section, but this time by following a WKB-type approach. This has the merit of leading to reasonably good approximations for both the smallest and second smallest eigenvalues of the boundary-value problem (2.14a)-(2.15a).

To simplify the algebraic manipulations, a change of independent variable is first introduced,

$$\rho := -x - k + \frac{1}{2} \qquad \Longrightarrow \qquad -k \le \rho \le 1 - k\,,$$

so that (2.14a) becomes

$$\frac{d^4W}{d\rho^4} + \mu\delta_0\frac{d}{d\rho}\left(\rho\frac{dW}{d\rho}\right) + \mu^2\delta_0 W = 0\,, \tag{6.1}$$

where we have written $\delta = \delta_0\mu$, with $\delta_0 = \mathcal{O}(1)$ – see the discussion at the end of §2. Note that under the above transformation the lower rim of the shell ($x = -1/2$) becomes $\rho = 1 - k$. Asymptotic approximations of the solutions of (6.1) can be sought in the form

$$W = U(\rho; \mu^{-1}) \exp\left(\mu^{1/2} \int^{\rho} p(\xi)\, \mathrm{d}\xi\right), \tag{6.2}$$

where $U \equiv U(\rho; \mu^{-1})$ and $p \equiv p(\rho)$ are to be found; the lower integration limit in (6.2) can be chosen to be any constant within the closed interval $[-k, 1-k]$. Substituting (6.2) into (6.1), and setting to zero the coefficients of like powers of μ, at leading order we discover the bi-quadratic

$$p^4 + \delta_0 \rho p^2 + \delta_0 = 0\,, \tag{6.3}$$

which has a pair of repeated roots when $\rho^2 = 4/\delta_0$. The positive solution of this equation is $\rho = \rho_0$, with

$$\rho_0 := \frac{2}{\sqrt{\delta_0}}\,; \tag{6.4}$$

ρ_0 defined above corresponds to one of the so-called *turning* (or *transition*) *points* of equation (6.1) – the negative value is irrelevant in the present case. Typically, the lower integration limit in the ansatz (6.2) is chosen to be ρ_0 (e.g., see [42, 45, 46, 47]).

Next, we note that the roots of (6.3) can be expressed in the following simplified form

$$p_1 = \begin{cases} \mathrm{i}\Omega_1^+ + \mathrm{i}\Omega_2^+\,, & \text{if} \quad \rho > \rho_0\,, \\ -\Omega_1^- + \mathrm{i}\Omega_2^-\,, & \text{if} \quad \rho < \rho_0\,, \end{cases} \qquad p_2 = \begin{cases} -\mathrm{i}\Omega_1^+ + \mathrm{i}\Omega_2^+\,, & \text{if} \quad \rho > \rho_0\,, \\ \Omega_1^- + \mathrm{i}\Omega_2^-\,, & \text{if} \quad \rho < \rho_0\,, \end{cases} \tag{6.5a}$$

$$p_3 = \begin{cases} -\mathrm{i}\Omega_1^+ - \mathrm{i}\Omega_2^+\,, & \text{if} \quad \rho > \rho_0\,, \\ \Omega_1^- - \mathrm{i}\Omega_2^-\,, & \text{if} \quad \rho < \rho_0\,, \end{cases} \qquad p_4 = \begin{cases} \mathrm{i}\Omega_1^+ - \mathrm{i}\Omega_2^+\,, & \text{if} \quad \rho > \rho_0\,, \\ -\Omega_1^- - \mathrm{i}\Omega_2^-\,, & \text{if} \quad \rho < \rho_0\,, \end{cases} \tag{6.5b}$$

where $\Omega_j^{\pm} \equiv \Omega_j^{\pm}(\rho)$ (for $j = 1, 2$) are defined below

$$\Omega_1^+ := \sqrt{\frac{\delta_0}{4}(\rho - \rho_0)}\,, \qquad \Omega_1^- := \sqrt{\frac{\delta_0}{4}(\rho_0 - \rho)}\,, \qquad \Omega_2^+ \equiv \Omega_2^- := \sqrt{\frac{\delta_0}{4}(\rho + \rho_0)}\,.$$

The behaviour of the roots of the bi-quadratic (6.3) as $\rho \to \rho_0^{\pm}$ is fairly easy to grasp with the help of these expressions – see Figure 10. For $\rho > \rho_0$, p_j ($j = 1, 2, 3, 4$) are purely imaginary and symmetrically placed with respect to the origin (since $\overline{p}_1 = p_3$ and $\overline{p}_2 = p_4$). When $\rho = \rho_0$, there are two pairs of coalescing roots, $p_1 = p_2$ and $p_3 = p_4$, with the characteristic roots still lying on the imaginary axis. Finally, as $\rho < \rho_0$ the roots split up in each of the four quadrants of the complex plane (but now $\overline{p}_1 = p_4$ and $\overline{p}_2 = p_3$). Similar turning-point problems have been studied by Steele [47] and Goldenweizer *et al.* [48]; in the context of other related wrinkling instability problems this situation was also encountered in our previous studies [38, 39].

Below, we take a more pragmatic approach than in the above references and provide an ad-hoc simplified asymptotic analysis for determining the eigenvalues of (6.1) subject to the boundary conditions stated in §2. A detailed analysis of the Stokes lines for the equation mentioned above indicates [49] that the usual quantization condition for the eigenvalues δ_0 involves *either* the pair of characteristic roots (p_1, p_2) *or* (p_3, p_4), but not both. This suggests that reasonable approximations

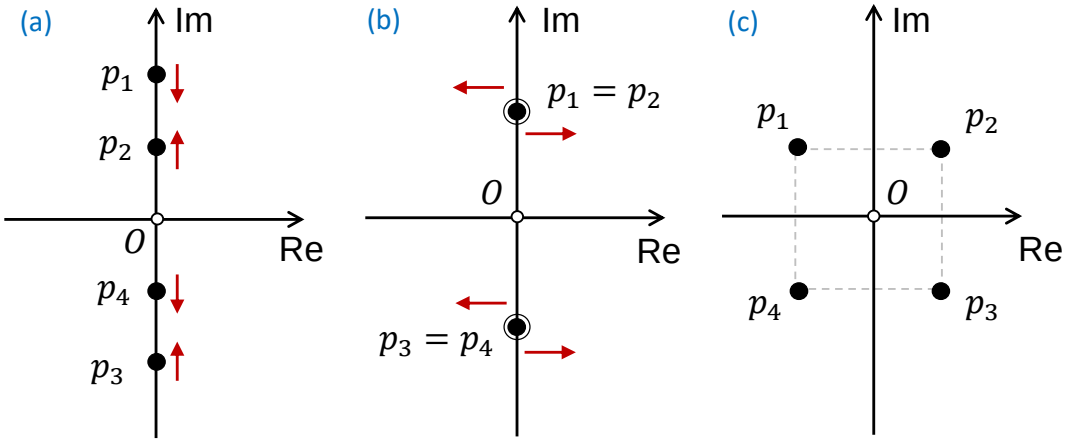

Figure 10: The behaviour of the charateristic roots $p_j \equiv p_j(\rho)$ $(j = 1, 2, 3, 4)$ of (6.3) as $\rho \to \rho_0^{\pm}$: (a) $\rho > \rho_0$; (b) $\rho = \rho_0$; (c) $\rho < \rho_0$. The arrows in (a) show how the positions of these roots change as $\rho \to \rho_0^-$, while in (b) they have a similar connotation corresponding to $\rho \to \rho_0^+$. The horizontal and vertical axes record the *real* ('Re') and *imaginary* ('Im') parts of the characteristic roots.

might be obtained by considering an associated second-order equation whose characteristic roots are $p = p_j(\rho)$ with $j = 1, 2$. Letting $\varepsilon := \mu^{-1/2}$, we consider the simplified differential equation

$$\varepsilon^2 \frac{d^2\overline{W}}{d\rho^2} - 2\mathrm{i}\varepsilon\Omega_2^+(\rho)\,\frac{d\overline{W}}{d\rho} - \frac{1}{2}\delta_0\rho_0\overline{W} = 0\,, \tag{6.6}$$

where, to avoid confusion, the unknown function is labelled $\overline{W}$ (instead of W); obviously, the presence of the complex coefficient requires $\overline{W} \equiv \overline{W}(\rho) \in \mathbb{C}$. The middle term in (6.6) is easily eliminated by making the usual change of dependent variable

$$\overline{W}(\rho) = V(\rho)\mathrm{e}^{-\eta(\rho)}\,, \qquad \eta(\rho) := -\mathrm{i}\varepsilon^{-1}\int_{\rho_0}^{\rho} \Omega_2^+(\xi)\,\mathrm{d}\xi\,, \tag{6.7}$$

where $V \equiv V(\rho) \in \mathbb{C}$ satisfies

$$\varepsilon^2 \frac{d^2V}{d\rho^2} + \left\{ \frac{1}{4}\delta_0(\rho - \rho_0) + \underline{\mathrm{i}\varepsilon\frac{d\Omega_2^+}{d\rho}} \right\} V = 0\,. \tag{6.8}$$

In this last equation we choose to disregard the underlined term, leading us to an Airy-type equation. To bring it into standard form we use the same transformation as already encountered a couple of times in the previous sections; in particular, we set $z \equiv z(\rho)$, with

$$z = a^{1/3}\rho + ba^{-2/3}\,, \qquad a := -\frac{1}{4}\varepsilon^{-2}\delta_0\,, \qquad b := \frac{1}{4}\varepsilon^{-2}\delta_0\rho_0\,,$$

so that the solution of the simplified equation (6.8) is simply $V = (1 + \mathrm{i})\mathrm{Ai}(z)$; we leave out the other function (i.e., $\mathrm{Bi}(z)$) because our interest is solely in solutions that have the requisite decaying properties mentioned in §3.

Assuming that the real and imaginary parts of the solutions of (6.6) are approximations for two linearly independent solutions of the original fourth-order equation (6.1), we can construct a linear

combination of these functions and then impose the boundary conditions $W = W'' = 0$ when $\rho = 1-k$. The corresponding determinantal equation can be shown to be

$$\mathrm{Ai}(z(\rho))\big[\underline{\varepsilon^{2/3}\mathrm{Ai}(z(\rho))} - 2^{4/3}\delta_0^{1/3}(\rho+\rho_0)\mathrm{Ai}'(z(\rho))\big]\Big|_{\rho=1-k} = 0\,. \tag{6.9}$$

By further discarding the underlined term in (6.9) we obtain $\mathrm{Ai}(z(1-k))\mathrm{Ai}'(z(1-k)) = 0$, which gives two options. If the first term in this product is zero then we recover an approximation for the second smallest eigenvalue $\delta_0 > 0$. The vanishing of the second term yields an approximation for the lowest eigenvalue. An outline of the main formulae is recorded below.

Reverting back to the asymptotic parameter $\mu \gg 1$, the equation $\mathrm{Ai}(z(1-k)) = 0$ gives

$$(1-k-\rho_0)^{3/2} = \zeta_0^{3/2}\rho_0\mu^{-1/2}\,, \tag{6.10}$$

and we recall that $\mathrm{Ai}(-\zeta_0) = 0$. Equation (6.10) can be used to find an asymptotic approximation for the turning point ρ_0. Routine calculations show that

$$\rho_0 = (1-k) - \zeta_0(1-k)^{2/3}\mu^{-1/3} + \frac{2\zeta_0^2}{3}(1-k)^{1/3}\mu^{-2/3} + \dots\,,$$

and an inversion of this result together with (6.4) lead to

$$\delta = 4(1-k)^{-2}\mu + 8\zeta_0(1-k)^{-7/3}\mu^{2/3} + \frac{20}{3}\zeta_0^2(1-k)^{-8/3}\mu^{1/3} + \dots \tag{6.11}$$

or, in terms of the original quantities from the references [23, 24] we also have

$$\lambda_L^{(II)} = \frac{1}{4}(1-k)^2\alpha^2\left[1 - 2\beta^{2/3}\zeta_0(1-k)^{-1/3}\alpha^{1/3} + \frac{7}{3}\beta^{4/3}\zeta_0^2(1-k)^{-2/3}\alpha^{2/3} + \dots\right]. \tag{6.12}$$

As already hinted by the notation employed in this last equation, the formula (6.12) represents an approximation for the second smallest positive eigenmode (i.e., not for the critical one). To explore the other possibility for satisfying the boundary constraint at the lower rim no new work is required. We can simply use (6.12) in which we change $\zeta_0 \to \zeta_0'$, with $(-\zeta_0')$ being the first zero of the derivative of the Airy function of the first kind, i.e. $\mathrm{Ai}'(-\zeta_0') = 0$, $\zeta_0' \simeq 1.0188$. For completeness, the relevant final formula is recorded below

$$\lambda_L^{(I)} = \frac{1}{4}(1-k)^2\alpha^2\left[1 - 2\beta^{2/3}\zeta_0'(1-k)^{-1/3}\alpha^{1/3} + \frac{7}{3}\beta^{4/3}\zeta_0'^2(1-k)^{-2/3}\alpha^{2/3} + \dots\right]. \tag{6.13}$$

An illustration of the excellent accuracy provided by the two asymptotic formulae (6.12) and (6.13) is recorded in Table 2. Both eigen-branches are approximated with relative errors that are roughly about $\mathcal{O}(10^{-4})$.

7 Discussion

In this study we have re-visited a simplified mathematical model for the self-buckling of symmetric equatorial spherical shell segments, previously proposed by Blum [23] and Blum & McComb [24]. An interesting aspect of their model is the partial support feature at the upper rim of the shell, which is fully controlled by a dimensionless parameter $0 \le k \le 1$ representing the proportion of the total weight supported there. For values of k close to the endpoints of this range, the eigenmodes of the

Table 2: Comparison of the asymptotic results (6.13) and (6.12) with the full numerical simulations of the original boundary-value problem defined in §2; the same notations as in Tab. 1 are employed here; also, $\beta = 7$ and $\alpha = 5 \times 10^{-7}$.

k	$\alpha^{-2}\lambda_L^{(I)}$ see (6.13)	$\alpha^{-2}\lambda_L^{(II)}$ see (6.12)	$\alpha^{-2}\lambda_{cr}^{(1)}$ (full numerics)	$\alpha^{-2}\lambda_{cr}^{(2)}$ (full numerics)
0.01	0.230980	0.214291	0.231080	0.214140
0.05	0.212519	0.196967	0.212540	0.196824
0.10	0.190532	0.176353	0.190539	0.176215
0.15	0.169752	0.156895	0.169830	0.156761
0.20	0.150179	0.138590	0.150183	0.138470

corresponding buckling problem were found to be localised near either the lower or the upper edges of the shell. Motivated by this observation, here we have focused primarily on two main asymptotic limits; one of them corresponds to $|k-1| = \mathcal{O}(1)$, while the other is characterised by $|k-1| \ll 1$. In each one of these two cases we have obtained simple and accurate asymptotic approximations for the non-dimensional spectral parameter $\lambda \equiv h^2/(12(1-\nu^2)R^2)$, where $R > 0$ is the radius of the spherical shell, ν denotes its Poisson's ratio, and h represents the shell thickness. The main asymptotic parameter used in our approximations was the quantity $0 < \alpha \equiv \gamma L/E \ll 1$, with γ being the specific weight of the shell material, E the Young's modulus, and L the height of the spherical segment (see Figure 1 in §1).

Taking advantage of the boundary-layer nature of the eigenmodes as $\alpha \to 0^+$, our approach has relied upon the general strategy developed in a number of our previous studies (e.g., [27, 29, 30, 38, 40]). However, the case when $|k-1| = \mathcal{O}(1)$ turned out to be more subtle than originally anticipated; despite the presence of two distinct branches of eigen-solutions that share the same leading-order term (i.e., an asymptotically double eigenvalue), the original multi-scale ansatz proposed in §5 – see equation (5.2), seems to have "missed" one of the eigen-branches. As a matter of fact, there is nothing wrong with the functional form of the proposed approximation; the reason for the incomplete results obtained therein is due to using only one of the boundary conditions, $W(Y) = 0$ for $Y = 0$. Given that the main differential equation (2.14) has real-valued coefficients, both the real and imaginary parts of (5.2) represent approximations for two linearly independent solutions of (2.14), so the leading-order asymptotic solution we are looking for will be of the form

$$W \simeq \left[\widetilde{c}_1 \cos\left(\mu^{1/6}\Omega Y\right) + \widetilde{c}_2 \sin\left(\mu^{1/6}\Omega Y\right)\right] \mathrm{Ai}(Z) + \ldots\,, \qquad (\widetilde{c}_1,\, \widetilde{c}_2 \in \mathbb{R})\,,$$

and it is this function that should be used in the boundary conditions $W = W'' = 0$ for $Y = 0$. The corresponding determinantal equation is $\mathrm{Ai}(Z)\mathrm{Ai}'(Z) = 0$ when $Y = 0$, and we are then led to either $\widetilde{\Gamma}_2\widetilde{\Gamma}_1^{-2/3} = -\zeta_0$ (the case already discussed in §5) or $\widetilde{\Gamma}_2\widetilde{\Gamma}_1^{-2/3} = -\zeta_0'$; the details of this latter case are very similar to what we have already done, so in the interest of brevity we do not pursue matters further here. We mention in passing that both approaches outlined in §5 and §6 are directly relevant to the drillstring buckling problems discussed in [50] (see also [22]).

Our analysis has been exclusively focused on the local asymptotic structure of the boundary value problem consisting of (2.14a) subject to (2.15a) when k is relatively far from the value $k_0 \equiv 1/4$. For such k-values, the results obtained in the preceding sections confirm that the piecewise smooth curve

$k \to \alpha^{-2}\lambda_{BM}(k)$ illustrated in Figure 2 is indeed a least upper bound for $\alpha^{-2}\lambda_{cr}$. Since we have two different sets of asymptotic expansions associated with $k \simeq 0^+$ and $k \simeq 1^-$, respectively, it would seem natural to inquire as to how those solutions morph into each other as k is gradually swept from 0 to 1 (or vice-versa), not least because the information reported by Blum [23] and Blum & McComb [24] appears to be contradictory. Indeed, in the former reference the curves $k \to \alpha^{-2}\lambda_{cr}(k)$ (for $0 \le k \le 1$) have a similar shape to the least upper bound curve seen in our Figure 2 but the corner is smoothed out (e.g., see Figure 10 in that report), while in the latter publication the sharp corner is present in all of the curves (e.g., see Figures 8-10 in [24]). These issues, together with a more detailed WKB analysis and several other aspects related to the present analysis, will be reported elsewhere.

A The coefficients C_j in equation (4.16)

The rather intricate expressions of the coefficients C_j ($j = 1, 2, \ldots, 6$) are recorded below for the sake of completeness. Letting

$$\omega := \frac{1}{2}(4k+1)^{-1}\left(k+\frac{1}{2}\right)^2 ,$$

all of these coefficients are of the form $C_j = \omega \widetilde{C}_j$, where

$$\widetilde{C}_1 := A_1\Gamma_1^{-2/3} + \zeta_0 A_2 \Gamma_1^{-1} , \qquad \widetilde{C}_2 := A_2\Gamma_1^{-1} , \qquad \widetilde{C}_3 := A_3\Gamma_1^{-1/3} ,$$

$$\widetilde{C}_4 := A_4 + \zeta_0 A_5\Gamma_1^{-1/3} , \qquad \widetilde{C}_5 := A_5\Gamma_1^{-1/3} , \qquad \widetilde{C}_6 := A_6\Gamma_1^{2/3} ,$$

and

$$A_1 := -\delta_2 + N_1^2 - 8N_1\zeta_0(4k+1)^{1/3}\left(k+\frac{1}{2}\right)^{-5/3} ,$$

$$A_2 := 32\zeta_0(4k+1)^{1/3}\left(k+\frac{1}{2}\right)^{-11/3} + 8N_1\left(k+\frac{1}{2}\right)^{-2}$$

$$A_3 \equiv A_5 := 4\left(k+\frac{1}{2}\right)^{-2} , \qquad A_6 := 1 ,$$

$$A_4 := -2N_1 - 8\zeta_0 k(4k+1)^{1/3}\left(k+\frac{1}{2}\right)^{-8/3} .$$

B The quantities involved in the solvability condition (5.15)

The coefficients d_{ij} are listed below

$$d_{00} := \zeta_0^2(1-k)^{-1/3} - \frac{1}{8}\delta_3(1-k)^{7/3} \equiv d_{00}^{(I)} - \delta_3 d_{00}^{(II)} ,$$

$$d_{01} := 2\zeta_0(1-k)^{-1/3} , \quad d_{02} := \frac{1}{8}(1-k)^{-1/3} , \quad d_{10} := 2d_{02} ,$$

$$d_{11} := -\zeta_0^2(1-k)^{-1/3} , \quad d_{12} := \frac{3\zeta_0}{4}(1-k)^{-1/3} , \quad d_{13} := -d_{02} .$$

Letting

$$I_0 := \int_{-\zeta_0}^{\infty} \mathrm{Ai}^2(Z)\,\mathrm{d}Z = \mathrm{Ai}_0'^2\,,$$

the integrals in the solvability condition (5.15) correspond to

$$\mathcal{J}_k := I_k/I_0\,, \qquad (k = 1, 2, \ldots, 6)\,,$$

$$I_1 := \int_{-\zeta_0}^{\infty} Z\mathrm{Ai}^2(Z)\,\mathrm{d}Z = -\frac{1}{3}\zeta_0\mathrm{Ai}_0'^2\,, \qquad I_4 := \int_{-\zeta_0}^{\infty} Z\mathrm{Ai}(Z)\mathrm{Ai}'(Z)\,\mathrm{d}Z = -\frac{1}{2}\mathrm{Ai}_0'^2\,,$$

$$I_2 := \int_{-\zeta_0}^{\infty} Z^2\mathrm{Ai}^2(Z)\,\mathrm{d}Z = \frac{1}{5}\zeta_0^2\mathrm{Ai}_0'^2\,, \qquad I_5 := \int_{-\zeta_0}^{\infty} Z^2\mathrm{Ai}(Z)\mathrm{Ai}'(Z)\,\mathrm{d}Z = \frac{1}{3}\zeta_0\mathrm{Ai}_0'^2\,,$$

$$I_3 := \int_{-\zeta_0}^{\infty} \mathrm{Ai}(Z)\mathrm{Ai}'(Z)\,\mathrm{d}Z = 0\,, \qquad I_6 := \int_{-\zeta_0}^{\infty} Z^3\mathrm{Ai}(Z)\mathrm{Ai}'(Z)\,\mathrm{d}Z = -\frac{3}{10}\zeta_0^2\mathrm{Ai}_0'^2\,,$$

where $\mathrm{Ai}_0' \equiv \mathrm{Ai}'(-\zeta_0)$, that is, the value of the derivative of the Airy function $\mathrm{Ai}(Z)$ at $Z = -\zeta_0$. The closed-form evaluation of these integrals was carried out with the help of the method proposed by Albright in [51, 52] (see also [53]).

References

[1] Brush, Don O., Almroth, Bo O.: Buckling of Bars, Plates, and Shells. John Wiley & Sons, Inc., New York (1975)

[2] Timoshenko, S.P., Gere, J.M.: Theory of Elastic Stability (2nd ed.). McGraw-Hill Book Company, New York (1961)

[3] Leipholz, H.: Stability of Elastic Systems. Sijthoff & Noordhoff, Alphen aan den Rijn, The Netherlands (1980)

[4] Greenhill, A.G.: Determination of the greatest height consistent with stability that a vertical pole or mast can be made, and of the greatest height to which a tree of given proportions can grow. Proceedings of the Cambridge Philosophical Society **4**, 65–73 (1881)

[5] Kanahama, T., Sato, M.: Mathematical modelling to determine the greatest height of trees. Scientific Reports **12**, 2039 (2022)

[6] Dargahi, M., Newson, T., Moore, J.: Buckling behaviour of trees under self-weight loading. Forestry: An International Journal of Forest Research **92**, 393–405 (2019)

[7] Fournier, M., Dlouha, J., Jaouen, G., Almera, T.: Integrative mechanics for tree ecology: beyond wood density and strength. Journal of Experimental Botany **64**, 4793–4815 (2013)

[8] Euler, L.: De altitudine columnarum sub proprio pondere corruentium.. Acta Academiae Scientiarum Imperialis Petropolitanae **1778**, 163-193 (1780)

[9] Panovko, Y.G., Gubanova, I.I.: Stability and Oscillations of Elastic Systems. Consultants Bureau, New York (1965)

[10] Wang, C.Y.: A critical review of the heavy elastica. International Journal of Mechanical Sciences **28**, 549–559 (1986)

[11] Atanackovic, T.M.: Stability Theory of Elastic Rods. World Scientific, Singapore (1997)

[12] Kerr, A.D.: The stability of a water tower. Ingenieur-Archiv **58**, 428–436 (1988)

[13] Cole, P.P., Abel, J.F., Billington, D.P.: Buckling of cooling-tower shells: bifurcation results. Journal of the Structural Division ASCE **101**, 1205–1222 (1975)

[14] Jullien, J.F., Aflak, W., L'Huby, Y.: Causes of deformed shapes in cooling towers. Journal of the Structural Division ASCE **120**, 1471–1488 (1994)

[15] Lim, C.W., Ma, Y.F.: Computational p-element method on the effects of thickness and length on self-weight buckling of thin cylindrical shells via various shell theories. Computational Mechanics **31**, 400–408 (2003)

[16] Billington, D.P.: Thin Shell Concrete Structures (2nd ed.). McGraw-Hill Publishing Company, New York (1990)

[17] Gould, P.L.: Analysis of Shells and Plates. Springer Verlag, Berlin, (1988)

[18] Gioncu, V., Ivan, M.: Buckling of Shell Structures (In Romanian). Editura Academiei Romane, (1978)

[19] Mitchell, R.F., Miska, S.Z.: Fundamentals of Drilling Engineering. Society for Petroleum Engineering, Richardson, Texas (2010)

[20] Bourgoyne Jr., A.T., Milheim, K.K., Chenevert, M.E., Young Jr., F.S.: Applied Drilling Engineering. Society for Petroleum Engineering, Richardson, Texas (2014)

[21] Belayneh, M.: A review of Buckling in Oil Wells. Shaker Verlag, Aachen (2006)

[22] Gulyayev, V., Glazunov, S., Glushakova, O., Vashchilina, E., Shevchuk, L., Shlyun, N., Andrusenko, E.: Modelling Emergency Situations in the Drilling of Deep Boreholes. Cambridge Scholars Publishing, Newcastle upon Tyne (2019)

[23] Blum, R.E.: Buckling of an equatorial segment of a spherical shell loaded by its own weight. MSc Thesis, Virginia Polytechnic Institute, Department of Engineering Mechanics, Blacksburg, Virginia (1966)

[24] Blum, R.E., McComb, H.G.: Buckling of an equatorial segment of a spherical shell loaded by its own weight. NASA Technical Note (TN D-4921), Washington D.C. (1968)

[25] Troger, H., Steindl, A.: Nonlinear Stability and Bifurcation Theory. Springer-Verlag, Wien (1991)

[26] van der Heijden, A.M.A.: Koiter's Elastic Stability and Structures. Cambridge University Press, Cambridge (2008)

[27] Coman, C.D.: Tensile bifurcations in a truncated hemispherical thin elastic shell. Zeitschrift für Angewandte Mathematik und Physik **71:178** (2020)

[28] Coman, C.D., Bassom, A.P.: Asymptotic limits and wrinkling patterns in a pressurised shallow spherical cap. Int. J. Non-linear Mech. **81**, 8–18 (2016)

[29] Coman, C.D., Bassom, A.P.: On the wrinkling of a pres-stressed annular thin film in tension. J. Mech. Phys. Solids **55**, 1601–1617 (2007)

[30] Coman, C.D., Bassom, A.P.: Boundary layers and stress concentration in the circular shearing of thin films. Proceedigs of the Royal Society of London A **463**, 3037–3053 (2007)

[31] Coman, C.D.: Continuum Mechanics and Linear Elasticity: An Applied Matematics Introduction. Springer Nature B.V., New York (2020)

[32] Gardner, D.R., Trogdon, S.A., Douglas, R.W.: A modified tau spectral method that eliminates spurious eigenvalues. Journal of Computational Physics **80**, 137–167 (1989)

[33] Gheorghiu, C.I.: Spectral Methods for Non-Standard Eigenvalue Problems. Springer Nature B.V., New York (2014)

[34] Boyd, J.P.: Chebyshev and Fourier Spectral Methods (2nd ed.). Dover Publications Inc., New York (2000)

[35] Lindsay, K., Rooney, C.E.: A note on compound matrices. Journal of Computational Physics **133**, 472–477 (1992)

[36] Ng, B.S., Reid, W.H.: The compound matrix method for ordinary differential systems. Journal of Computational Physics **58**, 209–228 (1985)

[37] Ng, B.S., Reid, W.H.: A numerical method for linear two-point boundary-value problems using compound matrices. Journal of Computational Physics **33**, 75–85 (1979)

[38] Coman, C.D.: Elastic instabilities caused by stress concentration. International Journal of Engineering Science **46**, 877–890 (2008)

[39] Coman, C.D., Bassom, A.P.: Wrinkling of pre-stressed annular thin films under azimuthal shearing. Mathematics and Mechanics of Solids **13**, 513–531 (2008)

[40] Coman, C.D., Bassom, A.P.: Singular perturbations and torsional wrinkling in a truncated hemispherical thin elastic shell. Journal of Elasticity **150**, 197–220 (2022)

[41] Nayfeh, A.H., Mook, D.T.: Nonlinear Oscillations. John Wiley & Sons, Inc., New York (1979)

[42] Cheng, H.: Advanced Analytic Methods in Applied Mathematics, Science, and Engineering. LuBan Press, Boston (2007)

[43] Coman, C.D.: Asymptotic approximations for pure bending of thin cylindrical shells. Zeitschrift für Angewandte Mathematik und Physik **68:82** (2017)

[44] Coman, C.D.: Localized elastic buckling: nonlinearities vs. inhomogeneities. IMA Journal of Applied Mathematics **75**, 461–474 (2010)

[45] Fedoryuk, M.V.: Asymptotic Analysis: Linear Ordinary Differential Equations. Springer Verlag, Berlin (1993)

[46] Northover, F.H.: Applied Diffraction Theory. American Elsevier Publication Company, New York (1971)

[47] Steele, C.R.: Application of the WKB method in solid mechanics. In : *Mechanics Today, Vol. 3*, S. Nemat-Nasser (Ed.), 243–295. Pergamon Press: New York (1976)

[48] Goldenweizer, A.L., Lidskii, V.B., Tovstik, P.E.: Natural Oscillations of Thin Elastic Shells (in Russian). Nauka, Moscow (1979)

[49] Coman, C.D.: WKB-type approximations for a self-buckling model. (unpublished manuscript)

[50] Musa, N., Gulyayev, V., Shlyun, N., Aldabas, H.: Critical buckling of drill strings in cylindrical cavities of inclined bore-holes. Journal of Mechanical Engineering and Automation **6**, 25–38 (2016)

[51] Albright, J.R.: Integrals of products of Airy functions. Journal of Physics A **10**, 485–490 (1977)

[52] Albright, J.R., Gavathas, E.P.: Integrals involving Airy functions. Journal of Physics A **19**, 2663–2665 (1986)

[53] Vallée, O., Soares, M.: Airy Functions and Applications to Physics. World Scientific, Singapore (2004)